Spectral evolution of two-layer weak geostrophic turbulence Part I: Typical scenarios

T. Soomere[1]

Max-Planck-Institut für Meteorologie, Bundesstrasse 55, D-20146 Hamburg, Germany

[1]On leave from the Estonian Marine Institute, Estonian Academy of Sciences, Tallinn, 1 Paldiski Road, EE0031 Estonia

Abstract. Long-time evolution of large-scale geophysical flows is considered in a β-plane approximation. Motions in an infinite 2-layer model ocean are treated as a system of weakly nonlinear Rossby waves (weak geostrophic turbulence). The evolution of the energy spectrum of the barotropic and the baroclinic modes is investigated on the basis of numerical experiments with the kinetic equation for baroclinic Rossby waves.

The basic features of free (nonforced inviscid) spectral evolution of baroclinic flows are similar to those of the barotropic motions. A portion of the energy is transferred to a sharp spectral peak while the rest of it is isotropically distributed. The peak corresponds to an intensive nearly zonal barotropic flow. Typically, this well-defined barotropic zonal anisotropy inhibits the reinforcement of its baroclinic analogy. For a certain set of initial conditions (in particular, if the barotropic zonal flow is not present initially), a zonal anisotropy of both modes is generated. The interplay between the multimodal nearly zonal flow components leads to the excitation of large-scale (several times exceeding the scale of the initial state), mostly meridional, baroclinic motions at the expense of the barotropic nearly zonal flow. The underlying mechanism is explained on the level of elementary mixed-triad interaction.

The whole wave field retains its essentially baroclinic as well as spectrally broad nature. It evidently tends towards a thermodynamically equilibrated final state, consisting of the superposition of a (usually barotropic, but occasionally multimodal) zonal flow and a wave system with a Raleigh-Jeans spectrum. This evolution takes place as a multi-staged process, with fast convergence of the modal spectra to a local equilibrium followed by a more gradual adjustment of the energy balance between the modes.

1 Introduction

1.1 A beta-plane model of synoptic motions

The synoptic motions on the Earth typically have a characteristic horizontal scale $L \gtrsim 100$ km, a vertical scale of the order of the full depth of the ocean (atmosphere), and a time scale of several dozen days. Their propagation may be described (to a first approximation) by treating the Earth's surface as an infinite flat plane (β-plane) in which the Coriolis parameter varies linearly in the North-South direction (e.g., Kamenkovich, 1977; Pedlosky, 1985). This approximation, although excluding the features associated with a countable set of wave harmonics on a sphere (e.g., Reznik et al., 1993) and the effect of the shores, greatly simplifies investigation into the equations of the motion. The mathematical description of synoptic-scale motions is reduced to a general problem of quasi-2D β-plane flows. In the pure barotropic case, their nondimensional equation reads

$$\partial(\Delta\psi - a^2\psi)/\partial t + \partial\psi/\partial x = \epsilon J(\Delta\psi, \psi), \qquad (1)$$

where ψ is the stream function, (x, y) - the Cartesian coordinates on the β-plane (the x-axis is directed to the East and the y-axis - to the North); t - time, $\epsilon = U/(\beta L^2)$ - the measure of nonlinearity; β - the North-South derivative of the Coriolis parameter, U - the characteristic velocity scale, $J(f, g) = f_x g_y - f_y g_x$ and a^{-1} - the Rossby radius. Eq. (1) coincides with the equation for drift waves in plasma (Hasegawa et al., 1979).

A principal difference of the motions in question as compared to the classical 2D turbulence (Kraichnan and Montgomery, 1980) consists in the presence of anisotropy. It is represented by the $\partial\psi/\partial x$ term and results in the existence of wave solutions to the linearized Eq. (1) called Rossby waves. Anisotropy is created owing to the interplay of the rotation and the sphericity of the Earth. The resulting variation of the Coriolis parameter distinguishes the preferred direction: the arbitrary rectilinear flow along parallels (zonal flow) described by $\psi = f(y)$ satisfies Eq. (1).

Correspondence to: T. Soomere

1.2 Kinetic approach

Natural motions usually consist of a vast number of harmonics. They can be treated as random wave fields with continuous spectral density (spectrum) of energy. Their evolution is governed by an infinite system of equations similar to the BBGKY system (Tapp, 1989) for their statistical moments. As a general rule, it cannot be truncated because of the incessant generation of the higher moments by the nonlinear coupling (Monin and Yaglom, 1975).

We shall concentrate on the *weakly nonlinear* particular case. Heuristically, for a weakly nonlinear field, nonlinear effects are negligible on time scales comparable with its characteristic period, but for longer time intervals nonlinearity may have a significant impact. Mathematically, such systems are described by equations [e.g., Eq. (1)] in which the nonlinear terms are small as compared to the linear ones. Physically, this means that the velocities of the particles involved in waves are small as compared to the phase velocities of wave harmonics. In this case, synoptic motions can be regarded as a system of weakly nonlinear Rossby waves (weak turbulence of Rossby waves or weak geostrophic turbulence).

A principal advantage of this restriction is that the fourth and higher order cumulants can be discarded (Hasselmann, 1962) in deriving an equation *(kinetic equation)* for the energy spectrum. This equation describes the slow (as compared to the characteristic wave period) spectral evolution of wave fields owing to the lowest-order resonant interactions. It is a hydrodynamical analogue of the Boltzmann equation, in which the colliding particles are represented by interacting wave packets. A formal difference here is that at least three packets must meet each other in order to interact. Travelling through each other during a short time interval (as compared to the time scale of spectral evolution), they execute an "elementary" interaction and propagate into various directions afterwards. These interactions are integrated by the kinetic equation in the same way as the Boltzmann equation integrates collisions of material particles.

1.3 Barotropic and baroclinic synoptic motions: numerical experiments and analytical results

The main features of barotropic motions on a β-plane or on a rotating sphere are summarized, e.g., in (Kraichnan and Montgomery, 1980; Rhines, 1979). With time, a clear dominance of the zonal component of the motion (usually intense zonal jets) is found to arise (Williams, 1978, among others). The jets are superposed by regions of mostly vortical motions. In terms of the energy spectrum, a well-defined peak in a certain area of the wave vectors arises, but the whole motion retains its spectrally broad nature. This behaviour results from the interplay of the β-effect and the nonlinearity. The former stabilizes motions with the dominating zonal component; the latter is responsible for widening the energy spectrum as well as for creating "strongly nonlinear" structures.

The basic theoretical features of the β-plane turbulence coincide with those of the isotropic $2D$ turbulence. Both motion systems possess two quadratic motion invariants - energy and enstrophy. The energy flux is directed to larger scales (the mean scale of motions increases with time) and the enstrophy flux towards smaller scales.

Predictions concerning the long-time evolution of the β-plane turbulence can be divided into two classes. First, the directionally averaged *nontruncated* spectra of *forced dissipative systems* should reach the classical $\kappa^{-5/3}$ or κ^{-3} laws within the inertial intervals (Rhines, 1975; Pelinovsky, 1977). Sazontov (1981; 1983) proved the formal existence of anisotropic power laws $k^\alpha l^\gamma$, where $\alpha, \gamma \in \mathbf{R}$, $\vec{\kappa} = (k, l)$ is the wave vector and $\kappa = |\vec{\kappa}|$. In a number of investigations into drift waves the system of motions is expected to decay into a zonal flow (e.g., Balk et al., 1990; Mikhailovsky et al., 1988). This belief has also been quite common in geophysics (e.g., Monin, 1990; Vallis, 1983).

Second, *free* (without energy sources and sinks) systems should evolve towards a "thermal" equilibrium state. In common with classical fields, which exhibit an ultraviolet catastrophe, the equilibrium statistical mechanics of these systems is meaningful only if the latter are *spectrally truncated*, i.e., include a limited set of wave harmonics, say, $0 \leq R_1 \leq \kappa \leq R_2 < \infty$. There exists a unique equilibrated energy distribution $F_{eq}^{-1} = a + b\kappa^2$ with two "temperatures" a, b (Kraichnan and Montgomery, 1980; Carnevale et al., 1981; Carnevale, 1982; Carnevale and Martin, 1982). Thus, the zonal anisotropy of geophysical flows may arise during a limited time interval and may finally be stirred (e.g., Salmon, 1980; Vallis and Maltrud, 1993).

Those predictions show fundamentally different directional structures of the final states. In the case of dissipative flows, a highly anisotropic scenario is believed to be true, while a perfect isotropy is expected to appear in the truncated inviscid case. This discrepancy can be resolved by showing that the β-effect occurs only in disequilibrium phenomena and does not affect the equilibrium mechanics (e.g., Holloway, 1986; Rhines, 1986).

The weakly nonlinear theory makes a step towards combining those scenarios. It predicts an anisotropic equilibrium state consisting of a superposition of a rectilinear zonal flow and a wave system with F_{eq} (Reznik and Soomere, 1983b). Physically, the existence of such states is a fine expression of an "equilibrium" between the impact of the β-effect and weak nonlinearity. This concept is supported by the results of numerical experiments with the kinetic equation for barotropic Rossby waves (Reznik and Soomere, 1983a; 1984a; 1984b; Reznik, 1986). A portion of the energy is always transferred to the zonal component of the flow. The rest of the energy is distributed more or less isotropically. The whole spectrum evidently evolves towards a specific distribution, consisting of the sum of a delta-shaped spectrum of a nearly zonal flow and an isotropic part (Fig. 1). Therefore, an intensive energy transfer to the zonal component of the motion by no means contradicts the fact that the system tends towards a thermodynamical equilibrium. However, the balance between the zonal and non-zonal components as well as the spectral shape of the equilibrium zonal flow still remains unclear. Further-
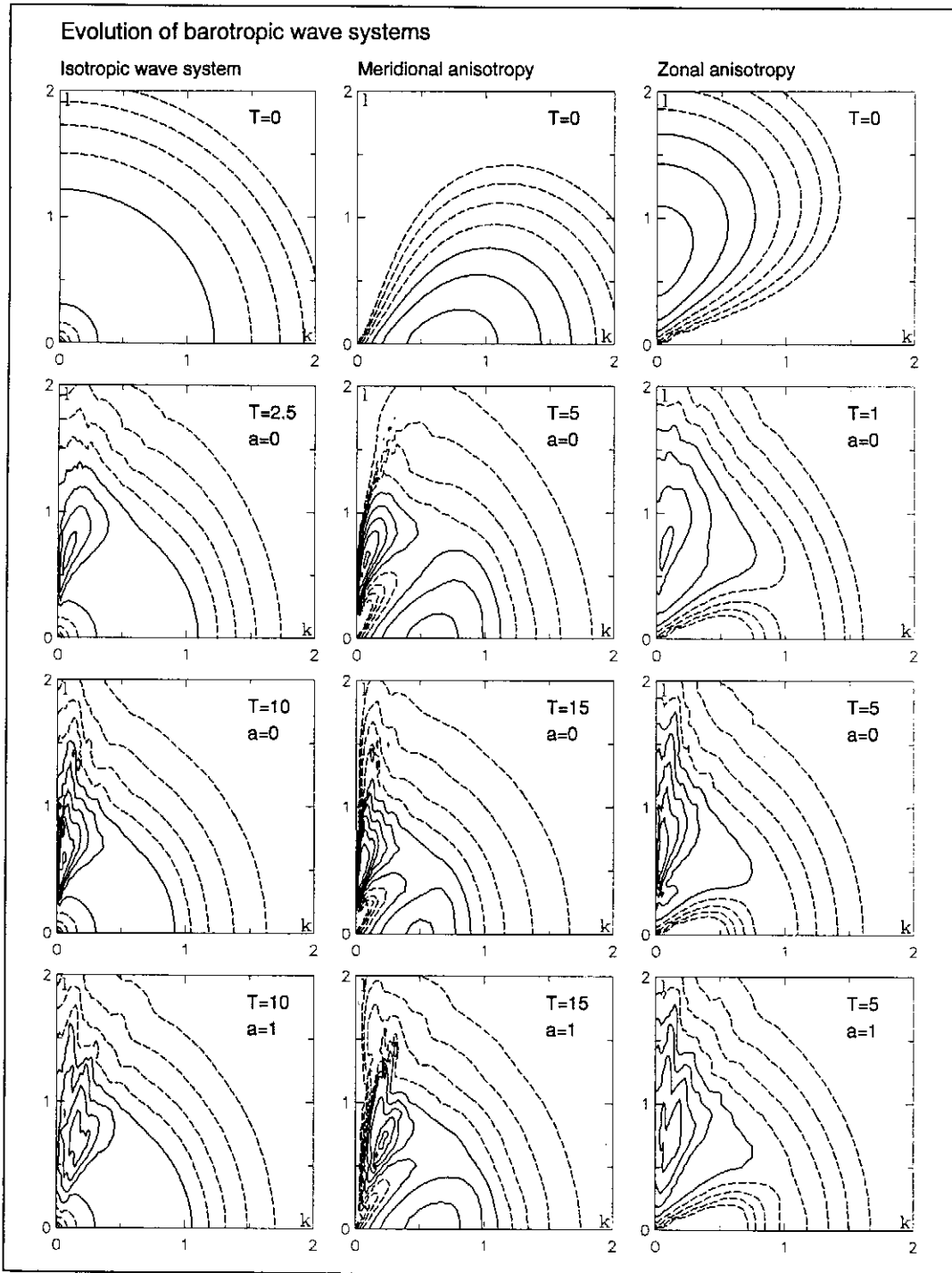
Fig. 1. Spectral evolution of barotropic Rossby wave systems. Interactions with waves with $\kappa < 4$ are ignored (Section 2.3). The sign of the k-component of the wave vector is reversed hereinafter. The initial states (the uppermost row) are normalized and spectrally isotropic (left column; spectrum is proportional to $\kappa \exp(-\kappa^2)$), with initially dominating meridional motion component (middle column; proportional to $\kappa \exp(-\kappa^2) \cos^4 \varphi$) or with initially prevailing zonal component (right column, proportional to $\kappa \exp(-\kappa^2) \cos^4 \varphi$). The Rossby radius $L_R = a^{-2} = \infty$ (medium rows) or $L_R = a^{-2} = 1$ (the lowest row). The main energy-containing area $0 \leq k, l \leq 2$ is represented in every panel. Contours are plotted in the logarithmic scale (four lines per decade at 1.0/1.78/3.16/5.62) starting from 0.01. Dashed lines show relatively small spectral level.

more, the exact equilibrium state cannot be reached owing to the inability of the resonant interactions to alter the zonal flow.

It is of interest that spectral pictures computed from different sources (direct numerical simulation, closure models with strong nonlinearity, weakly nonlinear framework) demonstrate a concordance (Vallis and Maltrud, 1993; Lee and Held, 1993; Reznik and Soomere, 1984a; Reznik, 1986). In all the listed cases, a strong medium-scale zonal anisotropy combined with a spectrally broad system of motion was detected. The described results are directly applicable to vertically homogeneous (barotropic) motions. However, synoptic motions are, as a rule, essentially depth-dependant (baroclinic). The vertical structure of stratified flows may be described in terms of a linear combination of a barotropic and a certain (maybe infinite) number of baroclinic modes (Phillips, 1966). This decomposition is equivalent to a model consisting of non-mixing vertically homogeneous layers. Since a substantial amount of the synoptic energy is usually contained in the two lowest modes, we shall use, to a first approximation, a two-layer model in which the motion contains only the barotropic and the (first) baroclinic vertical mode.

The basic features of the spectral evolution of barolinic motions on a β-plane coincide with those of the barotropic case. Energy mostly moves towards larger scales and enstrophy towards smaller scales (e.g., Salmon, 1980; Charney, 1971). However, a number of studies have shown that even the simplest baroclinic (2-layer) flows exhibit interesting new features. Significantly more intensive zonal flows have been detected, and an extraordinarily long time needed for obtaining statistical stationarity of the zonal flow was recorded in numerical experiments (Bartello and Holloway, 1991; Panetta, 1993; Vallis and Maltrud, 1993). The scale-increasing process is no longer universal and depends on details of the energy flux between the modes (Marshall, 1986). Within the kinetic theory a number of mathematical problems arise (Soomere, 1992; 1993). There exist different evolution scenarios of the energy balance between the motion components. Nontruncated forced (as well as realistic) systems are believed to fully barotropize (Rhines, 1977; Monin, 1990), while free truncated systems are expected to evolve towards an energy equipartitioning between modes (Salmon et al., 1976; Holloway, 1986).

The current study focuses on the effects of baroclinicity on the spectral evolution of free β-plane turbulence. It is mostly based on numerical experiments with the kinetic equation for Rossby waves in a 2-layer basin. A few typical runs will be presented in detail. A number of finer effects (balance between the generation of spectral peaks and spectral broadening, balance between the growth of a zonal flow and spectral isotropization, evolution towards thermodynamically equilibrated distributions and parameters of such distributions, details of energy and enstrophy fluxes) are presented only in short (and are hoped to be discussed in forthcoming papers). Although the study uses the parameters of synoptic motions in the oceans, the basic mechanisms apparently become evident also in the dynamics of the atmosphere.

Section 2 presents an introduction into the numerics of the kinetic description of baroclinic flows. Section 3 describes typical evolution scenarios. Section 4 discusses some details of energy redistribution mechanisms.

2 Numerics of the baroclinic kinetic equation

2.1 Baroclinic kinetic equation and its equilibrium solutions

Let us consider an infinite ocean of constant depth on an even β-plane consisting of two non-mixing homogeneous layers with densities $\rho_1 < \rho_2$ and mean thicknesses h_1, h_2, respectively. The subscript "1" corresponds to the upper layer, "2" - to the lower layer. Equations for stream functions ψ_1, ψ_2 within this model are analogous to Eq. (1) (see, e.g., Kamenkovich, 1977; Kamenkovich and Reznik, 1978; Pedlosky, 1985; Kozlov et al., 1987). The flow is decomposed into a barotropic $\Psi_0 = \psi_1 + s_0 \psi_2$ and a baroclinic $\Psi_1 = \psi_1 + s_1 \psi_2$ mode, where $s_0 > s_1$ are solutions of the equation

$$h_1 \rho_1 s^2 / \rho_2 + (h_1 - h_2)s - h_2 = 0.$$

The slow evolution of the spectral components is described by the following system of equations (Kozlov et al., 1987):

$$\frac{\partial F_p}{\partial \tau} = 8\pi \sum_{m,n=0}^{1} I_{pmn};$$

$$I_{pmn} = \int C_{\vec{\kappa}_1 \vec{\kappa}_2}^{pmn} K_{pmn} N_{pmn}^{-1} \delta(\omega_{pmn}^{012}) \delta(\vec{\kappa}_{012}) \, d\vec{\kappa}_{12}. \quad (2)$$

Here $F_p = F_p(\vec{\kappa}, \tau)$ is the spectrum of the barotropic ($p = 0$) or the baroclinic ($p = 1$) mode, $\tau = \epsilon^{-2}t$ - slow time, I_{pmn}, $p, m, n = 0, 1$ - collision integrals describing the energy alteration of the wave with $\vec{\kappa}$ of mode p due to interactions with waves belonging to modes m, n; $2C_{\vec{\kappa}_i \vec{\kappa}_j}^{pmn} = \gamma_{mn}^p |\vec{\kappa}_i \times \vec{\kappa}_j| \times (\kappa_j^2 + a_n^2 - \kappa_i^2 - a_m^2)$ - interaction coefficients; $\gamma_{mn}^p = (1 - 2|m - n|)(s_p + s_{1-m}s_{1-n})$; $K_{pmn} = C_{\vec{\kappa}_1 \vec{\kappa}_2}^{pmn} F_m^1 F_n^2 + C_{\vec{\kappa}\vec{\kappa}_1}^{npm} F_p F_m^1 + C_{\vec{\kappa}\vec{\kappa}_2}^{mpn} F_p F_n^2$; $F_p^m \equiv F_p(\vec{\kappa}_m)$, $N_{pmn} = (\kappa^2 + a_p^2)(\kappa_1^2 + a_m^2)(\kappa_2^2 + a_n^2)$; $\omega_p(\vec{\kappa}) = -k/(\kappa^2 + a_p^2)$ - dispersion relation of the Rossby waves of the p-th mode; $\omega_{pmn}^{012} \equiv \omega_p(\vec{\kappa}) + \omega_m(\vec{\kappa}_1) + \omega_n(\vec{\kappa}_2)$; $\vec{\kappa}_{012} \equiv \vec{\kappa} + \vec{\kappa}_1 + \vec{\kappa}_2$; $d\vec{\kappa}_{12} = dk_1 \, dl_1 \, dk_2 \, dl_2$, and the integrals are taken over the four-dimensional space $\mathbf{R}^2(\vec{\kappa}_1) \times \mathbf{R}^2(\vec{\kappa}_2)$. The quantities a_p^{-1} are equivalent to the barotropic ($p = 0$) and the baroclinic ($p = 1$) Rossby radii and equal to $a_p^2 = f_0^2[h_1^{-1} - \rho_1 s_p/(\rho_2 h_2)]/g'$, where f_0 is the mean value of the Coriolis parameter, g - gravity acceleration and $g' = g(\rho_2 - \rho_1)/\rho_2$. For simplicity, we shall call Eqs. (2) a baroclinic kinetic equation. It contains the simplest partial differential operator $\partial/\partial\tau$ and several integral terms I_{pmn} with quadratic nonlinearity. The unknown functions F_p both depend on slow time and two wave vector components. Each collision integral contains three Dirac delta functions and may be reduced to a one-dimensional integral. The delta functions reflect the fact that the most intensive energy exchange occurs between the wave harmonics the

170

wave vectors and frequencies of which satisfy the resonance conditions $\omega_{pmn}^{012} = 0$; $\vec{\kappa}_{012} = \vec{0}$.

A free wave system governed by a kinetic equation always conserves its energy, enstrophy and meridional component of the wave impulse [see below, Eqs. (5), (6), (7)]. Furthermore, an analogy [Eq. (8)] to Boltzmann's H-theorem (which proves the irreversibility of the spectral changes) holds. Thus, the systems in question evolve towards a thermodynamically equilibrated state. The corresponding solutions to the kinetic equation are called equilibrium solutions.

There exists only one family of differentiable equilibrium solutions $F_{peq}^{-1} = a + b(\kappa^2 + a_p^2)$ to Eqs. (2) (Kozlov et al., 1987). The equilibrium "temperatures" a, b are the same for both spectral components. These spectra coincide with the equilibrium spectrum of the isotropic $2D$ turbulence and are meaningful for spectrally truncated systems only. In common with the general geostrophic turbulence (Holloway, 1986), the final state of the spectral evolution of the flows in question is essentially baroclinic. Although in case $a_0 = 0$ there exists a pure barotropic solution $F_1 \equiv 0$ to Eqs. (2), the corresponding flow will evidently lose its energy to baroclinic disturbances.

The theory of anisotropic equilibrium solutions to the kinetic equation is generalized to the 2-layer case in (Kozlov et al., 1987). There exists a family of equilibrium solutions $F_{pzeq} = f_p(l)\delta(k) + F_{peq}$ to Eqs. (2). The continuous functions $f_p(l)$ representing the barotropic and baroclinic components of the zonal flow are independent, whereas the smooth parts of the spectra are related.

2.2 Reduction of the kinetic equation

Since the density of the water masses in the Earth's oceans varies insignificantly (it increases from surface to bottom typically by 0.5%), in Eqs. (2) it is allowed to disregard the quantities of the order of its alteration. We shall drop the terms $O((\rho_2 - \rho_1)/\rho_2)$ and replace ρ_1/ρ_2 by 1. These approximations yield (Kozlov et al., 1987):

$$
\begin{aligned}
s_0 &= h_2/h_1; \quad s_1 = -1; \\
a_0^2 &= \frac{f_0^2}{g(h_1 + h_2)}; \quad a_1^2 = \frac{f_0^2(h_1 + h_2)}{g' h_1 h_2}; \\
\gamma_{00}^1 &= \gamma_{01}^0 = \gamma_{10}^0 = 0; \quad \gamma_{00}^0 = \gamma_{01}^1 = \gamma_{10}^1 = s_0 + 1; \\
\gamma_{11}^1 &= s_0^2 - 1; \quad \gamma_{11}^0 = s_0(s_0 + 1).
\end{aligned}
$$

In particular, we obtain $I_{001} \equiv I_{010} \equiv I_{100} \equiv 0$, which reflects the fact that the interactions between two barotropic waves and one baroclinic wave in the oceans are much less intensive than other resonant interactions (Jones, 1979; Mirabel, 1985).

The natural boundary between the layers in the oceans is the main thermocline, usually located at a depth of $h_1 \sim 1$ km. The mean depth $(h_1 + h_2)$ of the ocean is approximately 5 km. With these values, the kinetic equation contains factors $(s_0 \pm 1)^2 \sim 30$, which can be removed by defining

$$
T = \tau(h_2/h_1 + 1)^2 = \tau(s_0 + 1)^2. \tag{3}
$$

By using (3), replacing F_0 by F and F_1 by $G = \alpha^2 F_1$, we obtain:

$$
\begin{aligned}
\frac{\partial F}{\partial T} &= 8\pi(I_{000} + \alpha I_{011}); \\
\frac{\partial G}{\partial T} &= 8\pi(1 - \alpha)^2 I_{111} + 16\pi I_{110},
\end{aligned} \tag{4}
$$

where $\alpha = h_1/h_2$ and the kernels of the collision integrals are modified in an obvious manner. Eqs. (4) have the same basic properties as Eqs. (2). Namely, the conservation laws for energy E, enstrophy Y and the meridional component of the wave impulse M as well as the law for the increase in entropy $H = \int \ln FG \, dk \, dl$, are satisfied:

$$
E = \int (F + \alpha G) \, dk \, dl = \text{const}; \tag{5}
$$

$$
Y = \int \left[(\kappa^2 + a_0^2)F + \alpha(\kappa^2 + a_1^2)G \right] dk \, dl = \text{const}; \tag{6}
$$

$$
M = \int \left[\frac{lF}{\omega_0(\vec{\kappa})} + \frac{\alpha l G}{\omega_1(\vec{\kappa})} \right] dk \, dl = \text{const}; \tag{7}
$$

$$
\frac{dH}{dT} = \frac{d}{dT} \int \ln FG \, dk \, dl \geq 0. \tag{8}
$$

Also, the sets of stationary and equilibrium solutions of Eqs. (2) and Eqs. (4) are identical.

The kinetic equation maintains spectral symmetry about the coordinate axes. A proof for the barotropic case given by Reznik and Kozlov (1981) can be easily generalized to the case in question. The tendency of barotropic spectra to move fast towards a symmetrical state (Reznik and Kozlov, 1981; Reznik and Soomere, 1984a) makes it natural to assume that an analogous mechanism also works in the baroclinic case. Below we shall consider only symmetrical initial spectra.

In order to remove the δ-functions from the collision integrals we perform integration over k_2, l_2 and then introduce the polar coordinates $\kappa, \varphi, \kappa_0, \varphi'$, where $\vec{\kappa} \equiv (\kappa \cos \varphi, \kappa \sin \varphi)$, $2\vec{\kappa}_1 = \vec{\kappa}_0 - \vec{\kappa}$; $2\vec{\kappa}_2 = -\vec{\kappa}_0 - \vec{\kappa}$; $\varphi' = \angle(\vec{\kappa}, \vec{\kappa}_0)$; $\kappa_0 = |\vec{\kappa}_0|$ (Longuet-Higgins and Gill, 1967). The argument of the remaining δ-function can be written as

$$
\omega_{pmn}^{012} = -k P_{pmn}/(16 N_{pmn}^{012}),
$$

where

$$
\begin{aligned}
P_{pmn} &= -16 N_{pmn}^{012} \omega_{pmn}^{012} (\kappa \cos \varphi)^{-1} = \\
&= \kappa_0^4 + 2A_{pmn}\kappa_0^2 + 4B_{pmn}\kappa_0 + C_{pmn}; \\
A_{pmn} &= 2(a_m^2 + a_n^2) + (\kappa^2 + 2a_p^2) \cos 2\varphi' - \\
&\quad - 2(\kappa^2 + a_p^2) \sin 2\varphi' \tan \varphi; \\
B_{pmn} &= 2(a_m^2 - a_n^2)\kappa^{-1} \times \\
&\quad \times [(\kappa^2 + a_p^2) \sin 2\varphi' \tan \varphi - a_p^2 \cos \varphi']; \\
C_{pmn} &= -3\kappa^4 - 4\kappa^2(a_p^2 + a_m^2 + a_n^2) \\
&\quad + 16 a_m^2 a_n^2 - 8 a_p^2(a_m^2 + a_n^2).
\end{aligned}
$$

The interaction integrals are reduced to

$$I_{pmn} = \sum_{\kappa_0 > 0:\, P_{pmn}(\kappa_0)=0} |k^{-1}| \int_0^{2\pi} \kappa_0 K_{pmn} \left| R_{pmn}^{-1} \right| \, d\varphi',$$

where $\kappa_0 = \kappa_0(\varphi')$ is a positive solution of the equation $P_{pmn}(\kappa_0, \varphi') = 0$ and

$$R_{pmn} = \frac{\partial P_{pmn}}{4 \partial \kappa_0} = \kappa_0^3 + A_{pmn}\kappa_0 + B_{pmn}.$$

Taking into account that in case $a_m = a_n$, we have

$$\int_0^{2\pi} \kappa_0 K_{pmn} \left| R_{pmn}^{-1} \right| \, d\varphi' = 2 \int_0^{\pi} \kappa_0 K_{pmn} \left| R_{pmn}^{-1} \right| \, d\varphi',$$

$\kappa_0 |R_{pmn}^{-1}| = \left| A_{pmn}^2 - C_{pmn} \right|^{-1/2}$ and $B_{pmn} = 0$, we can reduce the collision integrals of Eqs. (4) to

$$I_{000} = \int_0^{\pi} \frac{C}{64 \, |k| \, \sqrt{A_{000}^2 - C_{000}}} \times \qquad (9)$$

$$\times [2CF_1 F_2 - (C + D)FF_1 + (D - C)FF_2] \, d\varphi';$$

$$I_{011} = \sum_{\kappa_0 > 0} \int_0^{\pi} \frac{C}{64 \, |k| \, \sqrt{|A_{011}^2 - C_{011}|}} \times \qquad (10)$$

$$\times [2\alpha C G_1 G_2 + (4S - C - D)FG_1 + (D - C - 4S)FG_2] \, d\varphi';$$

$$I_{111} = \int_0^{\pi} \frac{C}{64 \, |k| \, \sqrt{A_{111}^2 - C_{111}}} \times \qquad (11)$$

$$\times [2C G_1 G_2 - (C + D)GG_1 + (D - C)GG_2] \, d\varphi';$$

$$I_{110} = \sum_{\kappa_0 > 0} \int_0^{2\pi} \frac{\kappa_0 (C - 2S)}{128 \, |kR_{110}|} \times \qquad (12)$$

$$\times [2(C - 2S)G_1 F_2 - \alpha(C + D)GG_1 + (4S - C + D)F_2 G] \, d\varphi'.$$

Here $2k_1 = \kappa_0 \cos(\varphi + \varphi') - \kappa \cos \varphi$; $2l_1 = \kappa_0 \sin(\varphi + \varphi') - \kappa \sin \varphi$; $C = \kappa_0^2 \kappa^2 \sin 2\varphi'$; $D = (3\kappa^2 - \kappa_0^2)\kappa_0 \kappa \sin \varphi'$ and $S = \kappa_0 \kappa \sin \varphi'(a_1^2 - a_0^2)$. Thus, we have reduced the collision integrals to integrals over a bounded interval. The arguments $\vec{\kappa}_1, \vec{\kappa}_2$ of the spectra lie on a specified curve called resonance curve.

2.3 Numerical method

A generalization of numerical treatment of the barotropic kinetic equation (Reznik and Kozlov, 1981; Reznik and Soomere, 1983a; 1984a) is used for the Cauchy problem for Eqs. (4). The spectra are computed at the nodes of a finite regular grid on the wave vector plane. In the case of a finite-enstrophy Rossby wave system $F_p \propto o(\kappa^{-4})$, thus, in the event of a sufficiently large computational region Ω, the truncation error should be small, at least during the initial phase of the simulations. The collision integrals are replaced by a quadrature formula and the values of the spectra at points not coinciding with the grid nodes are interpolated (Soomere and Rannat, 1991). Since the interaction coefficients for Rossby waves have a relatively simple form, the "straightforward" method is competitive with the "symmetrical" method proposed for surface waves (Hasselmann and Hasselmann, 1980; Hasselmann and Hasselmann, 1985; Hasselmann et al., 1985; Komen et al., 1994).

The rectangular grid consists of 49×66 nodes within the segment $\Omega = \{\kappa \leq 4, 0 \leq \varphi \leq \pi/2\}$ and is equivalent to the 97×114 grid used in the barotropic studies. The grid has a finer resolution in the vicinity of the l-axis. The singularity points of integrands (see next section) are initially computed and stored. The contributions from these are estimated on the basis of an asymptotic analysis of (Soomere, 1993). The quadrature method [ordinarily the Gauss' quadrature formula with 6 nodes in each segment $[m\pi/4, (m+1)\pi/4)], 0 \leq m \leq 7$] is modified as occasion requires within subintervals between the singularity points. The spectra at points $\vec{\kappa}_1, \vec{\kappa}_2$, not coinciding with the grid nodes, are interpolated (using a double linear interpolation method) between the nodes adjacent to $\vec{\kappa}_1, \vec{\kappa}_2$. Typically, the rms. error of the calculated collision integrals does not exceed 1%.

The resulting system of ordinary differential equations is not closed because in any finite region Ω there exist vectors $\vec{\kappa}$, interacting with vectors lying outside Ω. Two sorts of truncation were used in the barotropic experiments. First, the zero energy level (equivalent to infinitely fast dissipation) was assumed outside Ω. A disadvantage of this assumption is that the basic feature of irreversibility is lost. Another truncation scheme consists in completely ignoring all interactions involving vectors $\vec{\kappa} \notin \Omega$ and is equivalent to replacing the infinite integration area in Eq. (4) by $\Omega(\vec{\kappa}_1) \times \Omega(\vec{\kappa}_2)$. It ensures that all the conservation laws as well as the H-theorem remain valid. In what follows only a modification of the latter closure is used. By analogy with the barotropic case it can be expected that the main features of spectral evolution are insensitive with respect to the particular closure, at least in the main energetical area $\kappa \approx 1$. However, a comparative study of closures could be of interest.

Eqs. (4) were integrated by alternately using an explicit second-order Adams scheme (predictor) and an implicit third-order Adams scheme (corrector). Mostly, a value of the time step ΔT was used, for which one iteration of the corrector ensured the calculation of the spectra with a certain accuracy. The latter condition was always satisfied provided the

whole method remained stable. Numerical stability is ensured by the proper choice of the time step ΔT. There exists a critical value ΔT_{cr}, which depends on both the initial conditions and on the current time T. If $\Delta T < \Delta T_{cr}$, the method is practically insensitive with respect to the time step (a double decrease in the time step leads to an alteration of the main integral characteristics of an order of 10^{-5} per time unit). When $\Delta T \geq \Delta T_{cr}$, the calculation becomes unstable after a few steps. The critical value was estimated experimentally and the runs were mostly performed with $\Delta T \approx \Delta T_{cr}/2$.

An essential reason for the numerical instability is insufficient accuracy of computing the collision integrals, with several specific error components. First, the nodes of the quadrature formula are distributed regularly within the integration segment $[0, 2\pi]$ but usually very unevenly along the resonance curve. This property often results in a certain raggedness of the integrand. Second, the error of the interpolation procedure (which is negligible for the relatively smooth initial spectra) essentially increases when sharp spectral peaks arise (see below). Third, the length of the resonance curve crucially depends on the direction of the wave vector $\vec{\kappa}$ and varies more than by one order of magnitude for waves of equal length. A part of this curve often lies outside the computational area, resulting in a low resolution of the quadrature formula.

2.4 Applicability of the kinetic equation.

The kinetic equation is valid for limited time intervals ($T \lesssim \epsilon^{-2}$) and for limited wave vector areas ($\kappa \lesssim \epsilon^{-2}$). If T is of greater value, higher order interactions may become significant (Benney and Newell, 1969). For interactions of very short waves ($\kappa \gg \epsilon^{-2}$) the assumption of weak nonlinearity generally fails (Reznik, 1984; Reznik, 1986). The former restriction is apparently satisfied in our simulations, performed until $T = 5 \dots 15$. The latter is achieved through neglecting the interactions with short waves.

The integrals I_{000} and I_{111} are identical with the collision integral of the barotropic kinetic equation and are in no way extraordinary. Other integrals may contain singularities. Some of the barotropic waves cannot interact with the baroclinic mode (Jones, 1979), for them the equation $P_{pmn}(\kappa_0) = 0$ has no positive solutions and $I_{011} = 0$. The integrand of I_{011} has singularities, if any, only provided $\kappa^2 \leq 4/3$ (Fig. 2a). The singularities of I_{110} arise in an infinite area in the vicinity of the l-axis (Fig. 2b). Most of such singularities are integrable. A collision integral $I_{pmn}(\vec{\kappa})$ may diverge (equivalently, the kinetic equation may fail) if the function ω_{pmn}^{012} has multiple zeros on the surface $\vec{\kappa}_{012} = \vec{0}$. Generally, this equation is valid for the vector $\vec{\kappa}^*$ only provided that the quantity $\Delta = \left| \vec{\nabla}\omega_m(\vec{\kappa}_1) - \vec{\nabla}\omega_n(\vec{\kappa}_2) \right|$ has a nonzero lower boundary for all vectors $\vec{\kappa}_1, \vec{\kappa}_2$, resonantly interacting with $\vec{\kappa}^*$ (Reznik, 1984; Reznik, 1986). [For brevity, we shall speak of interactions of wave vectors, meaning wave interactions with these wave vectors; $\vec{\nabla} = (\partial/\partial k, \partial/\partial l)$ is the group velocity operator.] The case $\Delta = 0$ is called double resonance and the corresponding points $\vec{\kappa}^*$ in the wave vector space - double reson-
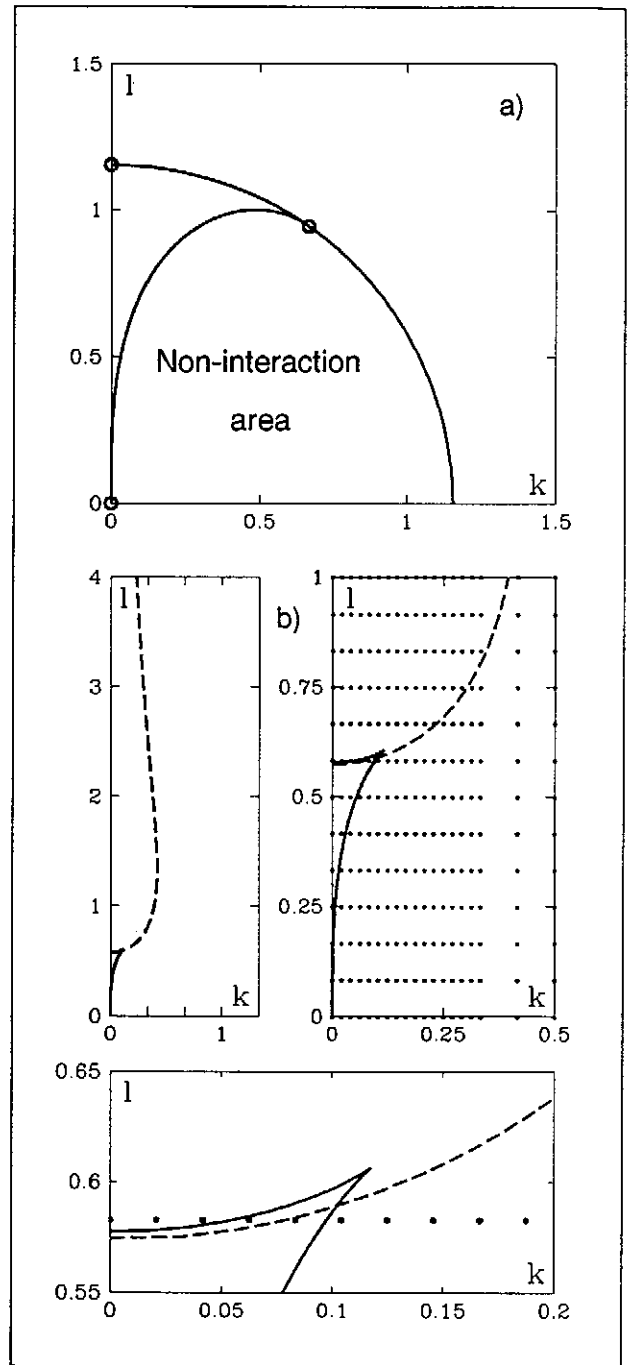

Fig. 2. Map of singularities of collision integrals for the case $a_0 = 0$; $a_1 = 1$.

a) Set of double resonance points for the barotropic mode (collision integral I_{011}). The small circles mark the singularity points of the double resonance curve. At its circular branch integral I_{011} converges. In the no resonance area interactions with the baroclinic mode are inhibited. Integrable singularities of the collision integral occur within the fishhook-like area between the double resonance curve and the l-axis.

b) Double resonance curve (bold line) and the area of singularities for the baroclinic mode (collision integral I_{110}). Singularities arise in the fishhook-like area (bounded by the double resonance curve and the l-axis) and in the infinite region between the l-axis and the triple resonance curve (dashed line; at this curve the function ω_{pmn}^{012} has a triple zero). Dots mark the grid used in simulations. For better comparison of the mutual location of the curves and grid points two enlargements are plotted.

ance points. It indicates that two harmonics of a resonance triad have equal group velocities and the underlying hypothesis of random phases does not apply.

The double resonance points for baroclinic Rossby waves form an algebraic curve on the (k, l)-plane called double resonance curve (Soomere, 1992). It always contains the l-axis and in the cases $a_p > a_m = a_n$ and $a_m \neq a_n$ also one or two closed branches (Fig. 2). Double resonance of waves with $k = 0$ has no impact on the total energy exchange and the kinetic equation remains valid in the vicinity of the l-axis (Reznik, 1986). It also remains correct in the neighbourhood of the k-axis as well as in the vicinity of the circular branch of the double resonance curve in the case $a_m = a_n$. For other double resonance points collision integrals generally diverge or remain undefined and the kinetic equation fails (Soomere, 1993).

The values of $\partial F/\partial T$, $\partial G/\partial T$ may be distorted in the vicinity of the double resonance curve. The total error caused by the inability of the kinetic equation to describe the energy exchange of "almost" double resonance waves is in a certain sense small in comparison with the integral intensity of nonlinear interactions (Soomere, 1993). That allows us to hope that in numerical experiments it is admissible to disregard the evolution of the spectrum in the vicinity of the double resonance curve and that the arising inaccuracy will not essentially distort the whole spectrum.

A set of experiments with the initial spectra of run 1 (see below) was performed in order to estimate the influence of such a distortion. At the grid points $\vec{\kappa}^*$, located in the neighbourhood of width ϵ_1 of the double resonance curve, the derivatives $\partial F/\partial T$, $\partial G/\partial T$ were approximated using their values at the grid points closest to $\vec{\kappa}^*$ located outside of this neighbourhood. On changing ϵ_1 from 0.005 to 0.1, the behaviour of the spectra, their derivatives and the basic integral characteristics remain practically unchanged until $T = 3$. That suggests that the distortion caused by double resonance apparently has no cumulative influence on the spectral evolution. Since no peculiar values of the spectra were detected in the test computations including all the grid points, we performed calculations with the complete grid. Also, the satisfactory temporal behaviour of the integral constraints (see next section) implicitly confirms that the effect of double resonance is negligible.

2.5 Experiments and their reliability

In this paper we shall mostly discuss results of runs $1 \ldots 9$, performed in order to generalize the results of barotropic simulations to the 2-layer case (Table B1). The initial energy distributions are proportional to $\kappa \exp(-\kappa^{-2})$ and occasionally contain spreading factors $\sin^4 \varphi$ or $\cos^4 \varphi$. Several runs were initially performed with a modest resolution of the quadrature formula (Soomere and Rannat, 1990; Soomere and Rannat, 1991) and repeated now with a greater accuracy.

Other simulations (runs $10 \ldots 21$) will be discussed in part II of this study. They cover the following subjects: generation of barotropic motions from pure baroclinic flows and evolu-
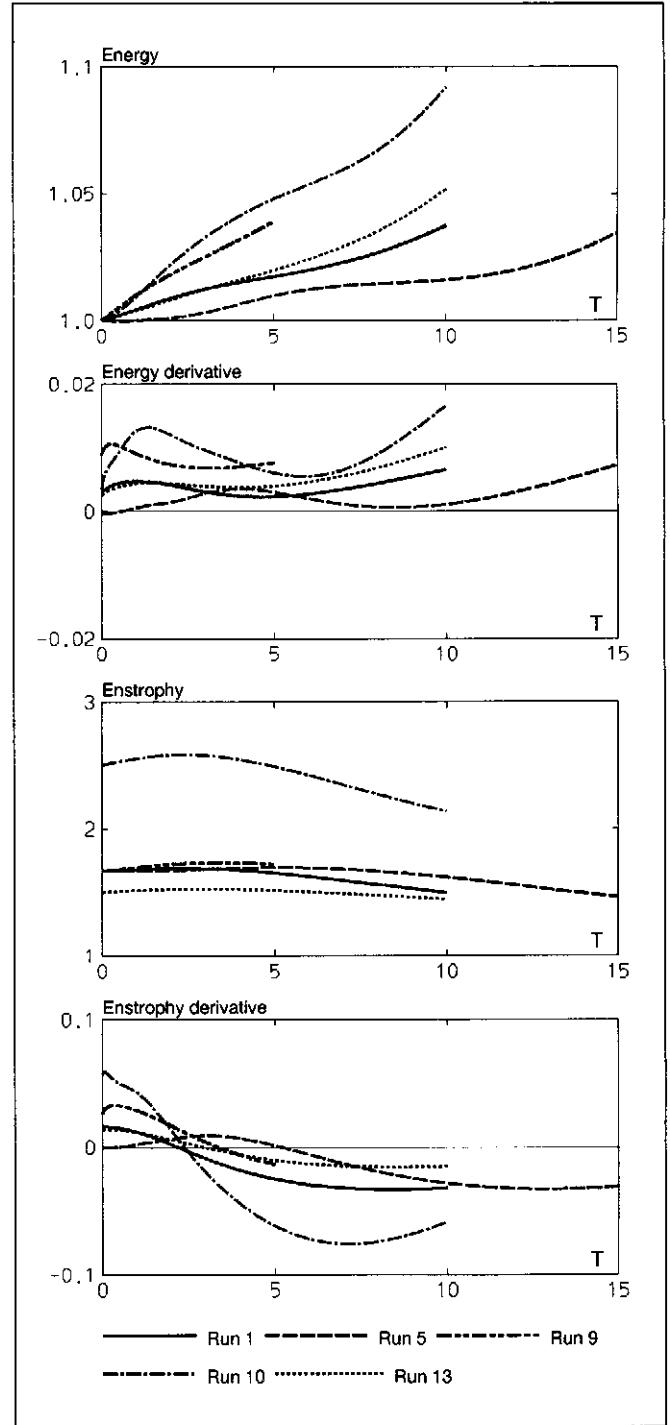

Fig. 3. Temporal behaviour of total energy, enstrophy and their derivatives. Runs 1 (both initial spectra isotropic), 5 (both with initial meridional anisotropy), 9 (both with initial zonal anisotropy), 10 (nearly barotropic isotropic initial state) and 13 (pure baroclinic isotropic initial state) are represented.

tion of barotropic flows in the presence of baroclinic disturbances (runs 10 ... 15), dependence of the spectral evolution on the vertical structure of motions (runs 16 ... 18) and the location of the initial spectral maximum (runs 19 ... 21).

The values of the parameters a_p are chosen as $a_0 = 0$; $a_1 = 1$ (i.e., the barotropic Rossby radius is infinite and the characteristic length scale L equals the baroclinic one). The parameter α (the ratio of the layers' thicknesses) is set at $\alpha = 0.2$ except for runs 16 ... 18. The initial total energy $E = 1$. A selection of the characteristics of the experiments is given in Table B1. A typical simulation consists of ca 1000 time steps and takes ca 2 hours of CRAY-2 single CPU time.

A permanent check is made on the proper operation of the scheme through the behaviour of the constraints [Eqs. (5), (6)] and the law of increasing in entropy [Eq. (8)]. The identity $M \equiv 0$ [Eq. (7)] is maintained numerically. Typically, the total energy E alters less than by 1% per time unit. At the beginning of most of the runs, the energy alteration rate $|\partial E/\partial T|$ is approximately 0.3% and somewhat increases in their final phases (Fig. 3, Table B1). It exceeds 0.01 only in a few experiments (runs 9, 12 ... 14, 17 ... 21; exceptionally, in run 15, $0.01 < |\partial E/\partial T| < 0.03$). However, the total interaction intensity in the listed simulations exceeds its typical value several times (see Table B1).

Apparently, the system enstrophy Y is more sensitive to computational errors because of the factor $\kappa^2 + a_p^2$ in its spectral representation. Since the spectra are evidently most distorted near the boundary of the computational area, the enstrophy flux towards shorter waves may be computed relatively inexactly. Indeed, the total enstrophy usually alters by 1 ... 2% per time unit. Its alteration rate ordinarily increases in the final phases of calculations, achieving in extreme cases (runs 15, 18 and 20) values $Y^{-1}\partial Y/\partial T|_{\max} = 0.04 ... 0.05$. Thus, the variation of both the constraints is quite satisfactory. As the Adams scheme conserves both the energy and the enstrophy, their behaviour indicates that with time the total accuracy of the quadrature and the interpolation procedures decreases to some extent.

Still another property that indirectly permits judging the operational correctness of the scheme is the total spectral width. In fact, nonlinearity should destroy spectral peaks and work towards widening the total spectrum (defocusing or spreading assumption). The spreading of an initially narrow wavenumber peak is intuitively reasonable and is commonly found in numerical simulations. For the barotropic case this assumption reads $E^{-1}[d\int(\kappa - \kappa_c)^2 F\,dk\,dl]/dT > 0$, where $\kappa_c = E^{-1}\int \kappa F\,dk\,dl$ is the spectral centroid (the mean wave number).

However, the effect of spectral widening is caused by the nonlinearity, which is now supposed to be small (as compared to the β-effect) and restricted to the specific geometry of resonant interactions. Nevertheless, in the barotropic experiments, the effect of spectral widening was observed in all cases in spite of the incessant generation of spectral peaks (Reznik and Soomere, 1984a).

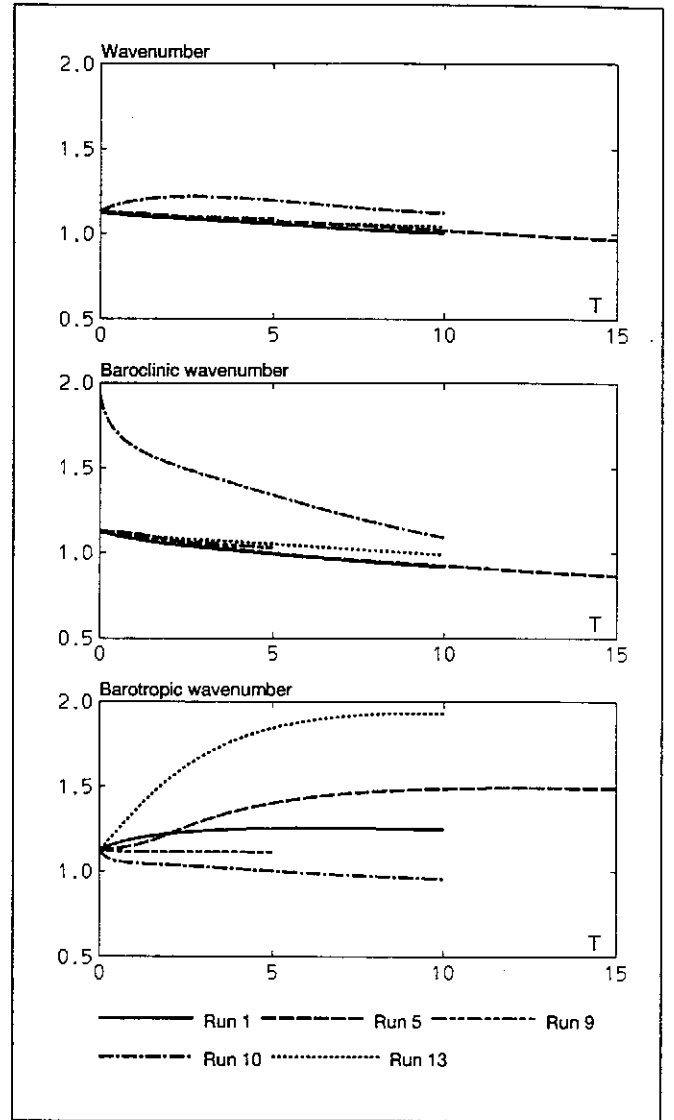We have used the following formulation of the spreading as-

Fig. 4. Temporal behaviour of spectral centroids of total energy (uppermost panel), barotropic mode (middle panel) and baroclinic mode (the lowest panel). Notations are the same as for Fig. 3.

sumption (Marshall, 1986):

$$\frac{\partial W}{\partial T} = \frac{\partial}{\partial T}\int \left[(\kappa - \kappa_{c0})^2 F + \alpha(\kappa - \kappa_{c1})^2 G\right]\,dk\,dl > 0, \quad (13)$$

where κ_{c0}, κ_{c1} are the spectral centroids of the barotropic and the baroclinic mode, respectively. In most of the experiments Eq. (13) holds true. Its slight violation occurs only in the final phases of runs 12 and 15, evidently owing to computational errors. (Both the energy and the total spectral width W increase in these cases, but the normalized values $W_n = W/E$ decrease.)

For inviscid nonforced $2D$ flows, the spreading assumption is equivalent to $d\kappa_c/dT < 0$, i.e. to the scale-increasing process (Merilees and Warn, 1975). Stratified motions possess an additional degree of freedom and even for 2-layer flows this assumption does not automatically yield a decrease in the

mean wave number. Let us start from the following formulation of the spreading assumption:

$$\frac{\partial}{\partial T} \int (\kappa - \kappa_{c0} - \kappa_{c1})^2 (F + \alpha G)\, dk\, dl > 0, \qquad (14)$$

where κ_{c0}, κ_{c1} are now normalized by using the total energy. From Eqs. (14), (5), (6) and the normalizing condition $E = 1$ we have that

$$\frac{\partial}{\partial T}(\kappa_{c0} + \kappa_{c1})^2 < -\partial E_1/\partial T, \qquad (15)$$

where E_1 is the baroclinic energy. Eq. (15) is a straightforward generalization of a result by Marshall (1986) stating that the total energy centroid $\kappa_c = \kappa_{c0} + \kappa_{c1}$ of a 2-layer β-plane flow must decrease only if the baroclinic energy increases. However, the latter condition is not always satisfied.

Figure 4 shows the temporal behaviour of the spectral centroids (the baroclinic and the barotropic centroids are normalized with the use of the energy of modes; the total centroid - with the total energy). In conformity with Eq. (15), κ_c decreases in all experiments showing energy conversion into the baroclinic form. Contrariwise, the mean wavenumber increases (in a part of runs 8, 13 . . . 15, 17) simultaneously with an intensive energy flow into the barotropic mode. Still we observe a general preference of the scale-increasing process. Namely, the mean swavenumber often decreases in spite of the energy flux into the barotropic mode (permanently in runs 1, 4 . . . 7, 9 and in a part of runs 8, 13 . . . 15, 17) and always in runs not revealing any considerable energy exchange between the modes.

Thus, an energy cascade to smaller scales appears only simultaneously with an intensive energy conversion to the barotropic form and is evidently restricted to special types of flows. An analogous phenomenon is mentioned by Rhines (1977; 1979) as a scenario consisting in the generation of small-scale baroclinic vortices at the expense of large-scale baroclinic flows. In realistic quasi$-2D$ turbulence this process may temporarily block or weaken the inverse energy cascade. However, such an anomalous cascade evidently appears during extreme events when baroclinic energy considerably exceeds its equilibrium level.

It should be noted that all the initial fields have small amplitudes of the waves with $\kappa \gg 1$. Hence, their evolution toward an equilibrated distribution is accompanied by an energy transfer from the area $\kappa \sim 1$ to shorter waves. Further on, in the course of time quite powerful spectral peaks arise (see below). It is remarkable that the spreading assumption as well as very often an increase in the scale hold true.

3 Typical scenarios

3.1 Generation of a barotropic nearly zonal flow as a major scenario

Let us track some typical examples of spectral evolution. First let us look at the evolution of the initial spectra

$$F(\vec{\kappa}, 0) = G(\vec{\kappa}, 0) = p\kappa \exp(-\kappa^2) \sin^4 \varphi \text{ (run 9). Here}$$
$p = 16/[3\pi^{3/2}(1 + \alpha)(1 + p')]$ is the normalizing factor, $p' = \operatorname{erf}(4) - 1 \sim 10^{-7}$, and $\operatorname{erf}(x)$ is the probability integral. The correction term p', arising from the truncation in use, is evidently negligible as compared to computational errors and will be omitted hereafter. The initial conditions correspond to a system of motions with predominating zonal components of both modes. Simulation was performed until $T = 5$. During the experiment, the intensity of interactions I [see Eq. (17)] decreases more than 17 times as compared to its value at $T = 0$ and the system entropy attains a practically constant level.

We found interesting behaviour of both the spectra and their time derivatives (Fig. 5). The evolution of the *barotropic mode* resembles that of the 1-layer case (Reznik and Soomere, 1984a). At $T = 0$ curves $\partial F/\partial T = 0$ divide the $\partial F/\partial T$ field into four parts. Areas of energy inflow I, III are placed near the l- and the k-axis, respectively. Although the maximum values of $\partial F/\partial T$ in the relatively narrow area I exceed those in area III, the latter is much greater and gains more energy than area I. Physically, that distribution supports a spectrally narrow almost-zonal flow with $l \sim 1$ and a mostly meridional flow with $k \sim 1$ with a wide spectrum. The former process generates an extremely sharp and high barotropic spectral peak in the vicinity of the l-axis at $\kappa \approx 0.6 . . . 0.7$. As the peak corresponds to a nearly zonal flow, we call it a zonal peak. The latter process decreases in intensity and apparently only adjusts the spectrum F to an isotropic state remote from the l-axis.

The absolute values $|\partial F/\partial T|$ in area II exceed those in area IV by at least one order of magnitude; thus, the latter does not play any essential role in the energy exchange. Area II contains two local minima at $\kappa \approx 0.5$ and $\kappa \approx 1.3$. The former is probably connected with initial zonal anisotropy since it does not appear in runs with other initial distributions of barotropic motions. Its disposition does not alter significantly during the experiment. At $T \approx 2$ the latter extremum shifts closer to the l-axis, into the area covered by the zonal peak. This peculiarity causes an "erosion" process of the upper right slope of the zonal peak, a typical phenomenon in all the experiments. It additionally enhances the steepness of the slope and evidently adjusts the peak towards a delta-like cusp.

In the course of time the values of $|\partial F/\partial T|$ decrease all over the wave vector plane. Areas I, III decrease as well and a new inflow area V remote from the origin splits off from area III. Area II increases to some extent and stretches out along the l-axis. These topological changes have a negligible influence on the spectral evolution in all the experiments and hereafter we shall omit the minor details of the derivative fields.

At the outset, the evolution of the *baroclinic mode* is characterized by an intensive energy inflow at $l \lesssim 1$ (area I of the distribution $\partial G/\partial T$) and an energy outflow at $l \gtrsim 1$ (area II). Energy exchange in areas III and IV is negligible. Area I has two inflow maxima (similar to those in areas I and III of the $\partial F/\partial T$ field) corresponding to the reinforcement of both the nearly zonal flow and the mostly meridional disturbances. The former process rapidly ceases and the baroclinic
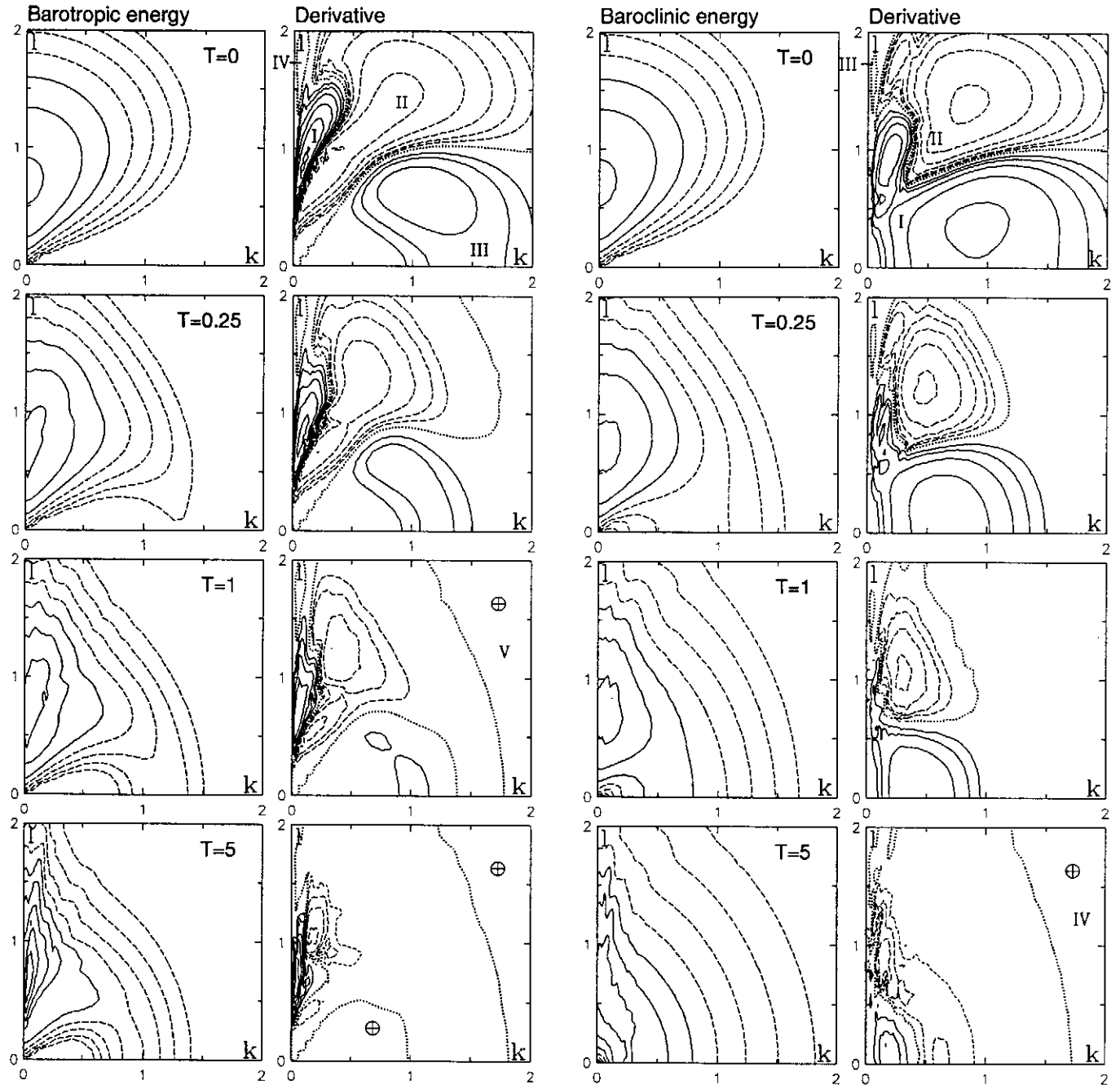
Fig. 5. Temporal evolution of energy spectra and their time derivatives. From left: evolution of the barotropic spectrum and its derivative; evolution of the baroclinic spectrum and its derivative.

Initial conditions are $F(\vec{\kappa}, 0) = G(\vec{\kappa}, 0) = p\kappa \exp(-\kappa^2)\sin^4 \varphi$, $16p^{-1} = 3\pi^{3/2}(1+\alpha)$ (run 9). Contours are plotted in the logarithmic scale (four lines per decade: 1.0/1.78/3.16/5.62) starting from ± 0.01. Dashed lines in the left column correspond to smaller values of spectrum; in the right column - to negative values of the temporal derivative. Dotted line marks curves $\partial F/\partial T = 0$, $\partial G/\partial T = 0$. Area $0 \le k, l \le 2$ is represented in every box. Inflow and outflow areas with no plotted contours are marked by symbols $\oplus$ or $\ominus$, respectively. Areas are numbered according to references in text. An additional short-dashed contour at $\partial F/\partial T = -0.00562$ or $\partial G/\partial T = -0.00562$ is plotted at $T = 5$.
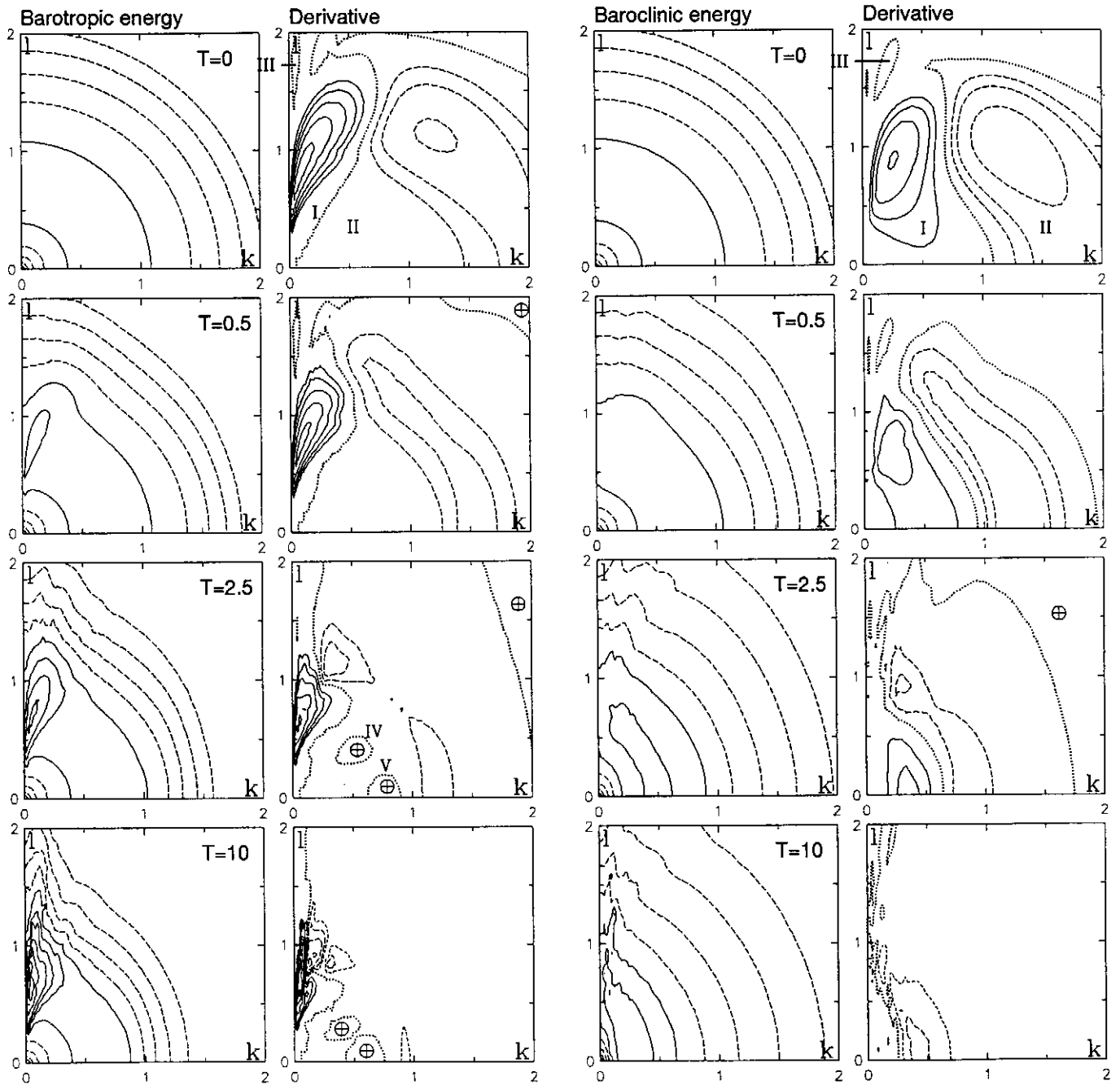
Fig. 6. As for Fig. 5, but for isotropic initial functions $F(\vec{\kappa}, 0) = G(\vec{\kappa}, 0) = p\kappa \exp(-\kappa^2)$, $2p^{-1} = \pi^{3/2}(1 + \alpha)$ (run 1). An additional short-dotted contour at $\partial F/\partial T = -0.00562$ or $\partial G/\partial T = -0.00562$ is plotted at $T = 10$.

zonal flow is suppressed starting from $T \approx 0.5$. Differently from the barotropic mode, the latter process remains active during whole the experiment (there permanently exists an intensive inflow region close to both the k-axis and the origin). The resulting spectrum is nearly isotropic, whereby the isotropization process acts much faster than in the barotropic case. Baroclinic energy mostly flows along the l-axis, while both in the 1-layer experiments and in the case of the barotropic mode energy exchange mainly occurs between waves nearly equal in length.

Consider also the evolution of a spectrally isotropic initial state $F(\vec{\kappa}, 0) = G(\vec{\kappa}, 0) = p\kappa \exp(-\kappa^2)$, $2p^{-1} = \pi^{3/2}(1 + \alpha)$ (run 1; Fig. 6). Both the distributions $\partial F / \partial T$ and $\partial G / \partial T$ initially contain a small region of intensive energy inflow I near the l-axis and a large outflow region II. Areas III-V of weak outflow or inflow are dispensable. Thus, at the outset, barotropic and baroclinic medium-scale zonal motions are both supported at the expense of all other wave harmonics.

Barotropic energy outflow region II mostly increases with time. It is accompanied by an initial decrease in the maximum values for $|\partial F / \partial T|$ until $T \approx 0.8$ and by a transition of their location from $\vec{\kappa} \approx (1.2, 1.2)$ to $\vec{\kappa} \approx (0.2, 1.2)$. The inflow region gradually shrinks, and towards the end of the calculation it forms only a narrow band in the neighbourhood of the l-axis. The maximum values for $\partial F / \partial T$ in it mostly increase to some extent. In the course of time their location shifts to the origin and somewhat approaches the l-axis. This leads to the formation of a high peak near the l-axis. The transition of the energy outflow maximum causes, as above, its erosion in the final phase of the experiment. Remote from the l-axis, spectrum F preserves a more or less isotropic shape.

Outflow region II for the $\partial G / \partial T$ field initially somewhat decreases in size. Starting from time $T \approx 1.5$ it expands and occupies, as in the case of $\partial F / \partial T$, nearly all the computational region. Simultaneously, the outflow maximum shifts closer to the l-axis and starts to stir the zonal anisotropy. Differently from the barotropic evolution, the energy inflow region is compressed towards the k-axis. The initial inflow maximum near the l-axis only leads to a temporary increase in the zonal component of the baroclinic mode. Towards the end of the simulation, the baroclinic spectrum obtains a nearly isotropic shape.

The temporal evolution of the time derivatives of both the spectra is similar to either of the described scenarios in all the runs with comparable initial energies of both modes (runs 2 ... 8; also some other experiments). They always initially reveal a characteristic two-lobed (or three-lobed, in the case of initial zonal anisotropy only) structure with an intensive inflow area close to the l-axis. However, towards the end of simulations, energy is mostly transferred into the barotropic nearly zonal flow and (occasionally) into large-scale baroclinic meridional motions.

The evolution of the barotropic mode is always similar to that in the 1-layer experiments (Reznik and Soomere, 1984a; 1984b; Reznik, 1986). A portion of the energy is transferred into a zonal peak, while the rest of the spectrum tends to become isotropic. The peak is placed between $l \approx 0.3$ and $l \approx$

1.0, has its minimal width near to the origin, widens to some extent at medium wavenumbers and has the universal form of an elongated hogback. It has abrupt slopes near to the origin, an enlargement near its maximum at $\kappa \approx 0.7$ and a gently sloping end at $\kappa \approx 1$. The isotropization process is the fastest in the case of medium scale processes ($\kappa \approx 1 \ldots 1.5$), but less evident for short and long waves (see below, Figs. 10, 12). At $\kappa \ll 1$ the interaction coefficients tend to zero as κ^4, decelerating the whole evolution process. For smaller scales, energy transfer can be distorted owing to the limited computational area $\{\kappa \leq 4\}$.

Typically, the baroclinic spectrum soon takes a practically isotropic shape and/or preserves it until the end of the experiments. Thus, resonant interactions always form a powerful spectrally narrow barotropic zonal flow but usually do not affect the zonal component of the baroclinic mode.

In order to check the further behaviour of such systems, we continued runs 1 and 5 during extra 5 nondimensional time units (in addition to the data listed in Table B1). The barotropic spectral peak keeps increasing and concentrates with time in an ever narrower vicinity of the l-axis, but there appears no sign of baroclinic zonal anisotropy.

3.2 Role of intermodal interactions

Since Eq. (3) introduces a new time scale, the quantitative features and the time units of the current study are not directly comparable with the 1-layer case. The previous section also reveals a few major deviations from the barotropic scenario, obviously caused by intermodal interactions. First, the baroclinic zonal flow is typically not excited. Second, baroclinic meridional motions are supported to some extent. Third, although the increase in the Rossby radius causes a shift of the zonal peak closer to the l-axis, as well as a certain increase in its amplitude (Reznik and Soomere, 1984a; Fig. 1), the extremely high amplitude of the barotropic zonal flow apparently does not result from the assumption that $a_0 = 0$ only.

The current model contains three types of interactions. Two of them (involving waves belonging to a fixed mode, called self-interactions and integrated by collision integrals I_{000} and I_{111}) are identical to interactions of the 1-layer flow. The third class is formed of mixed triads consisting of one barotropic and two baroclinic harmonics (intermodal interactions). They are responsible for both the energy flux between the modes and an additional energy redistribution within the modes. Triads containing one baroclinic and two barotropic waves are neglected (Section 2.2).

Let us examine the energy fluxes created by self- and intermodal interactions. First, the results of run 9 (Fig. 7).

At $T = 0$ the fields of self-interactions of both the spectral components $\partial F_{si} / \partial T$, $\partial G_{si} / \partial T$ resemble those in the barotropic experiments. Minor differences between them result from the difference of the Rossby radii and from the weight $(1 - \alpha)^2 = 0.64$ at the integral I_{111}. The intensity of barotropic self-interactions exceeds that of the baroclinic mode more than twice and the main inflow area for the barotropic mode is concentrated in the narrower neighbourhood of the
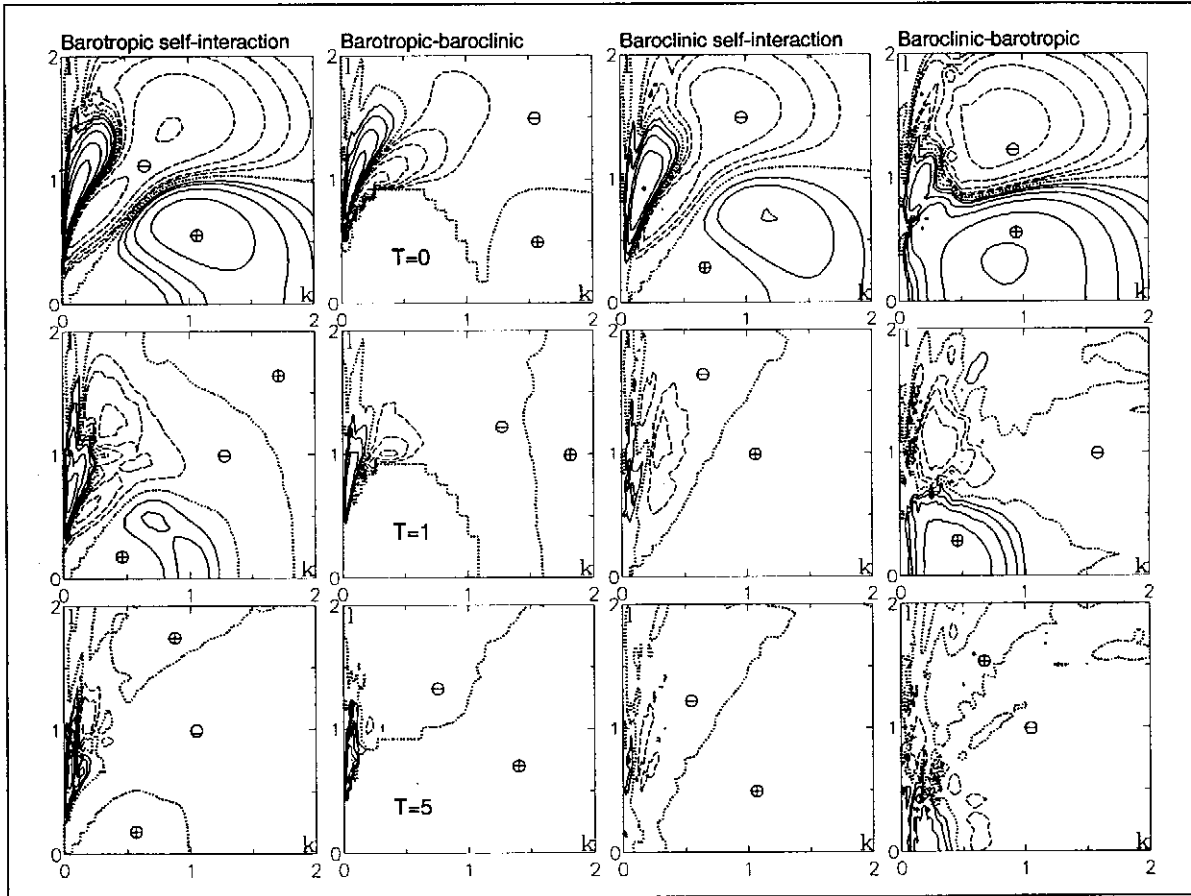
Fig. 7. Instantaneous fields of spectral fluxes created by self- and intermodal interactions for run 9. In the columns the following distributions are drawn (from left to right): self-interaction of the barotropic mode $\partial F_{si}/\partial T$, interactions of the barotropic mode with the baroclinic harmonics $\partial F_{ii}/\partial T$, self-interaction of the baroclinic mode $\partial G_{si}/\partial T$, interactions of the baroclinic mode with barotropic harmonics $\partial G_{ii}/\partial T$. Contours are plotted in the logarithmic scale (four lines per decade: 1.0/1.78/3.16/5.62) starting from ± 0.01. Dashed lines correspond to negative values of the derivative components; dotted line–their zero values. Area $0 \leq k, l \leq 2$ is represented in every box. Symbols $\oplus$ and $\ominus$ mark inflow and outflow areas, respectively.

l-axis.

Their further evolution, however, shows hardly any concurrence. On the one hand, the evolution of the $\partial F_{si}/\partial T$ field resembles that of the barotropic simulation: both inflow areas decrease and move closer to the l-axis while the outflow area (with two relative minima) widens. Towards the end, the inflow area close to the k-axis practically disappears, but the analogous area close to the l-axis maintains its intensity. In other words, after a "saturation" of the meridional flow components, energy is gradually transferred to a nearly zonal flow. On the other hand, the intensity of the baroclinic self-interactions $\partial G_{si}/\partial T$ falls rapidly, no prevailing energy flow being observed during the later phase of the experiment. At $T = 0$ the total energy flux between the modes

$$
\begin{aligned}
I_{FG} &= 8\pi \int I_{011}\, dk\, dl = -16\pi \int I_{110}\, dk\, dl \\
&= dE_0/dT = -dE_1/dT
\end{aligned}
$$

is of the order of 5% of the total interaction intensity I (see below), decreases rapidly, and remains small until the end of the experiment. Thus, intermodal interactions result rather in energy redivision within the modes than in the creation of an intermodal energy flux. The field of $\partial F_{ii}/\partial T$ (describing the interactions of the barotropic mode with the baroclinic harmonics) vanishes in the non-interaction area (Fig. 2) and remains small in the vicinity of the k-axis during the whole computational time. The remainder of it is qualitatively similar to the field of $\partial F_{si}/\partial T$. A relatively narrow inflow area is located in the neighbourhood of the l-axis. A wide outflow area covers most of the (k, l)-plane. At the outset, it has a tongue-like extension between the inflow area and the non-interaction area. The tongue is narrow and it does not prevail in the integral energy transfer, but its presence results in a steepening of the barotropic spectral peak. With time, it shortens and nearly disappears at $T \approx 1.5$. Therefore, intermodal interactions unnoticeably affect mostly meridional barotropic motions but essentially amplify the barotropic zonal flow. For this particular run, the absolute values of $\partial F_{ii}/\partial T$ are, as a rule, smaller than the values of $\partial F_{si}/\partial T$ during the whole simulation, except in the closest vicinity of the l-axis.

At $T = 0$ the field of $\partial G_{ii}/\partial T$ consists of two main parts roughly divided by the line $l = 1$. The energy flux is directed from the area $l > 1$ into the area $l < 1$ (i.e., to mostly meridional flow components). The inflow area contains an extension near the l-axis, which corresponds to a weak tendency to amplify the nearly zonal flow. Since typically $|\partial G_{ii}/\partial T| > |\partial G_{si}/\partial T|$, intermodal interactions mostly determine the baroclinic energy alteration. Indeed, the temporal evolution of the $\partial G_{ii}/\partial T$ field resembles the behaviour of the total derivative $\partial G/\partial T$. In the course of time, its extremes move closer to both the l-axis and the origin. The extension of the inflow area along the l-axis recedes and soon disappears. Further on, the energy transfer mainly tends to stir the initial zonal anisotropy and to create a peak near the k-axis.

The described features of self- and intermodal interactions are qualitatively common for all the runs with initially comparable energies of the modes. An initially two-lobed structure as represented in Fig. 8 is also possible. The majority of the energy redistribution for the barotropic mode takes place owing to its self-interactions, the field of which is always similar to that in the 1-layer simulations. They support the nearly zonal flow, which is additionally reinforced owing to intermodal interactions. Contrariwise, the behaviour of the baroclinic mode is mostly governed by intermodal interactions, which mainly support meridional flow components. Baroclinic zonal anisotropy is generated only at the outset. As time goes on, mixed interactions destroy it and amplify large-scale non-zonal motion components.

The intensity of baroclinic self-interactions decreases more rapidly than that of other interaction types (Figs. 7, 8). From the barotropic experiments it follows that the tendency towards a zonal anisotropy ceases only for systems, close to the thermal equilibrium (Reznik and Soomere, 1984a; 1984b). Thus, intermodal interactions apparently force the baroclinic component towards a local equilibrium $G^* = (a^* + b^* \kappa^2)^{-1}$ (with "temperatures" a^*, b^* not necessarily coinciding with those of the actual final state).

3.3 Generation of two-modal nearly-zonal flow

Obviously, the spectrally isotropic evolution of the baroclinic mode cannot be an overall feature of the motions in question. For example, in the case of a pure baroclinic initial flow, intermodal interactions are initially small and the baroclinic zonal anisotropy should be generated, at least, during some time interval. This is demonstrated by integrating the initial states with the mostly meridional anisotropy of the barotropic mode (run 6; Fig. 9).

In such cases, the evolution of the barotropic mode and its derivative is in no way extraordinary (cf. Fig. 1). Also, it has many common features with the evolution of initially isotropic systems (only the smallest outflow area III lacking and inflow areas IV,V are replaced by a prolongation of the main inflow area I; cf. Fig. 5). With time, a typical high and sharp zonal peak emerges while the rest of the energy apparently tends to an isotropic distribution.

However, both the initial and the further evolution of the baroclinic mode are similar to that of the barotropic mode. At the outset, the derivative $\partial G/\partial T$ contains a well-defined maximum in the vicinity of the l-axis in inflow area I. Its other peak is located close to the k-axis and expresses a tendency to support non-zonal flow components. Further on, outflow area II gradually widens and later embraces most of the computational area. Area III is dispensable and areas IV,V show up temporarily.

With time, the derivative field permanently manifests an intensive baroclinic energy inflow close to the l-axis. Correspondingly, a baroclinic zonal peak emerges near the l-axis and continues to grow during all the computational time. Its disposition and geometrical features are analogical to those of the barotropic one. However, it is somewhat lower and wider
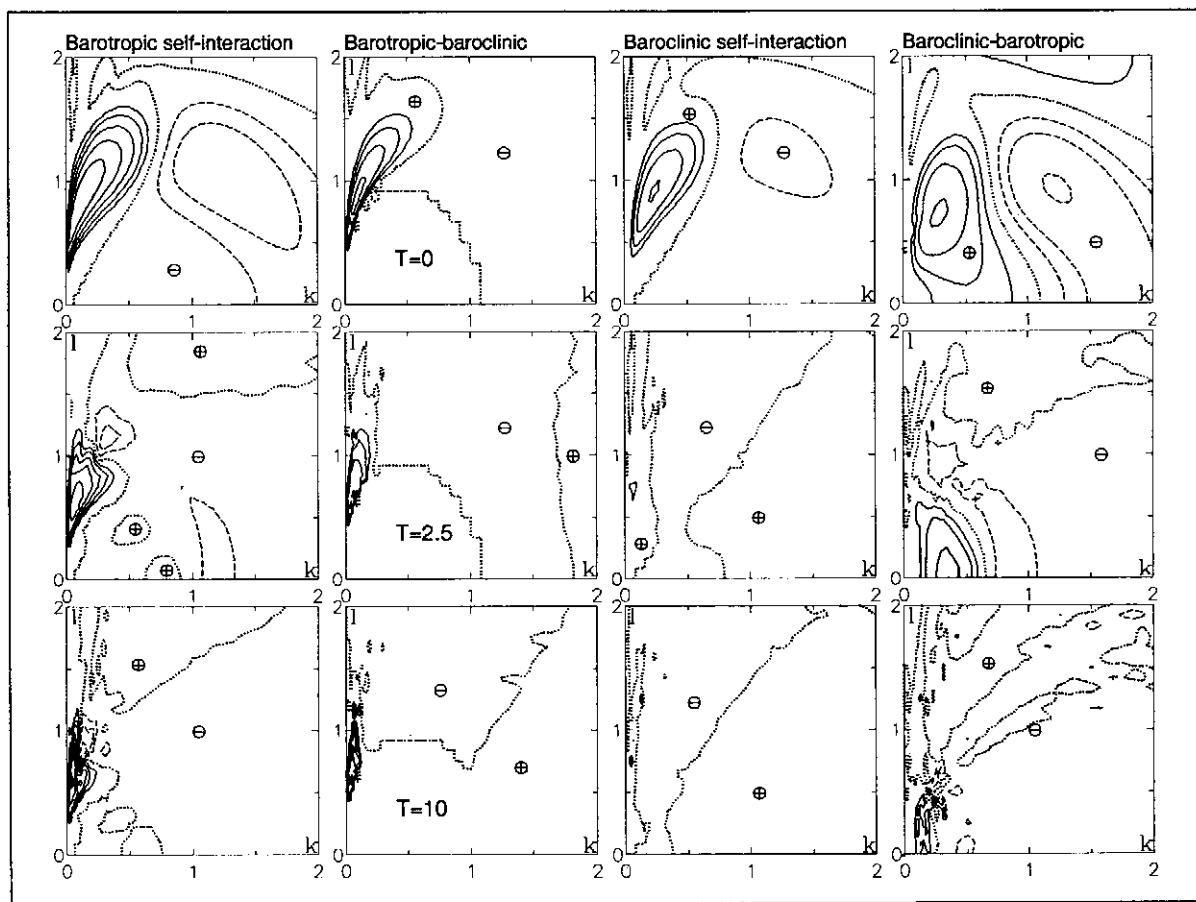
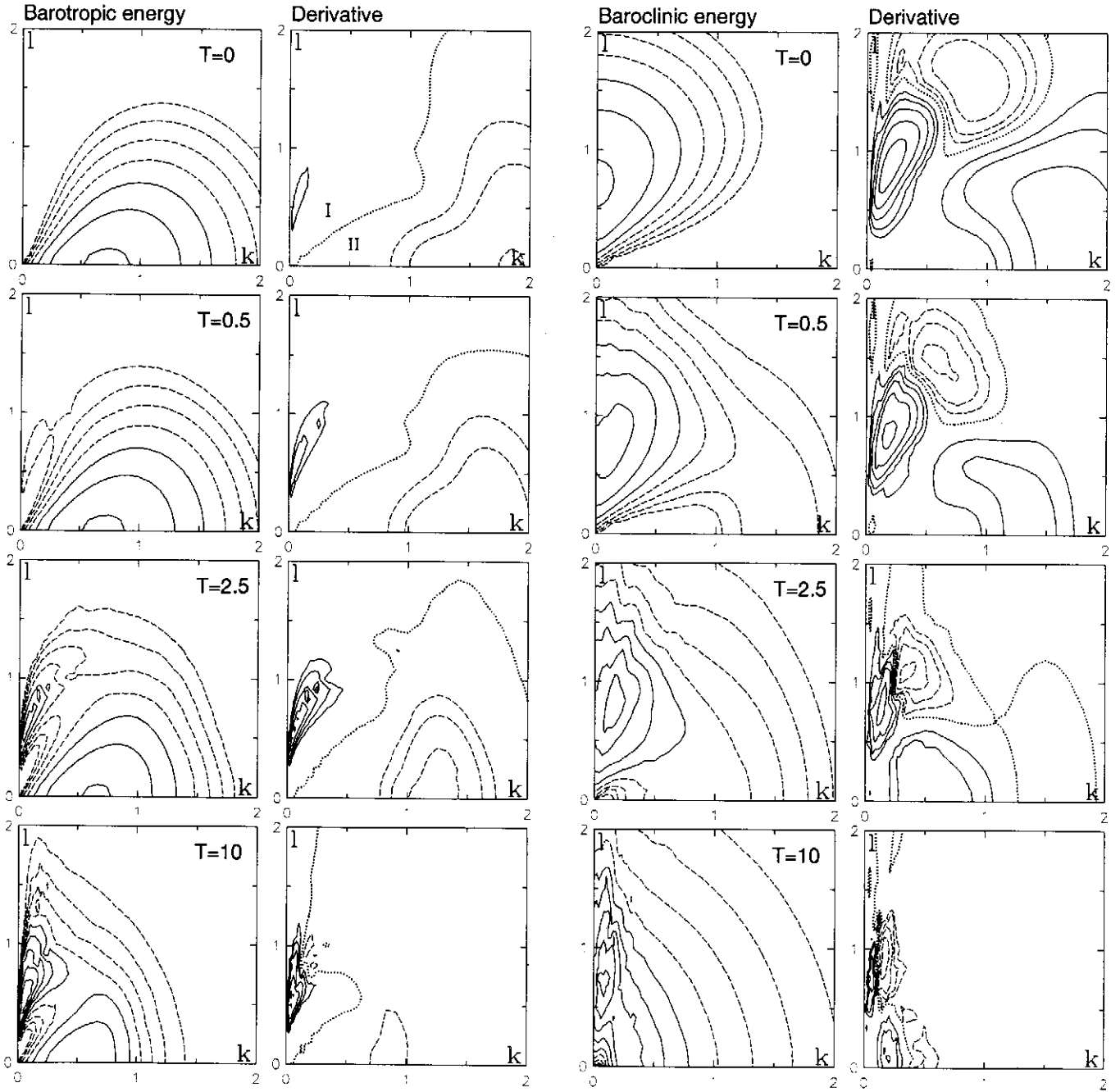**Fig. 8.** As for Fig. 7, but for run 1.

Fig. 9. As for Fig. 5, but for run 6 with the initial functions $F(\vec{\kappa}, 0) = p\kappa \exp(-\kappa^2) \cos^4 \varphi$; $G(\vec{\kappa}, 0) = p\kappa \exp(-\kappa^2) \sin^4 \varphi$; $16p^{-1} = 3\pi^{3/2}(1 + \alpha)$.
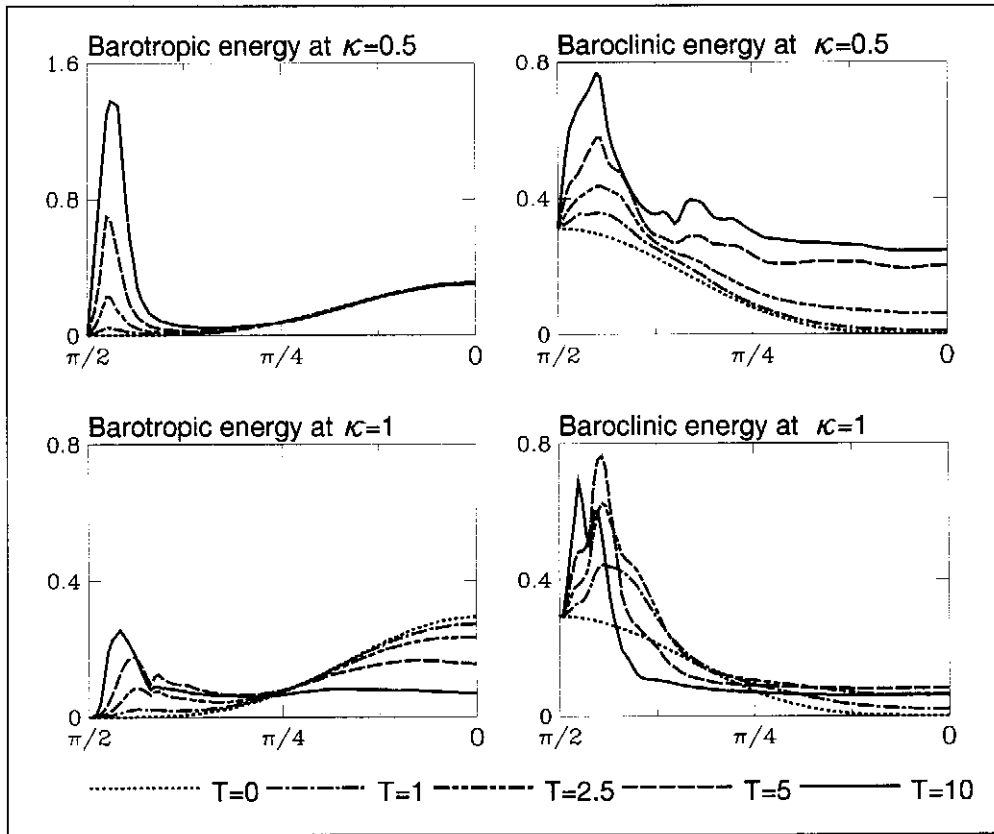
Fig. 10. Behaviour of barotropic (left) and baroclinic (right) spectra at the lines κ=const. The results of run 6 are given. Note the evidence of the "erosion" process of the baroclinic zonal peak at $\kappa = 1$, as well as the nearly perfect isotropy of the baroclinic spectrum at $\varphi \leq 3\pi/4$, $T \geq 5$.

than the barotropic one, has slightly shelving slopes, is placed at a greater distance from the l-axis (Fig. 10) and, in general, is similar to that of the 1-layer experiments with the Rossby radius $a_R = 1$ (Fig. 1).

Therefore, the modal structure of the zonal flow turns out to be strongly dependent on the initial state. For forced dissipative systems, as might be encountered in nature, this fact is counter-intuitive. However, for the irreversible case in question it is somewhat unexpected. It can be interpreted as a temporary feature, but apparently it is related to the indeterminated structure of the equilibrated zonal flow.

As in (Panetta, 1993), this feature may show that the concept of full barotropization is only applicable to particular flow types. Usually, the barotropic zonal flow will be excited faster and after some time will "inhibit" the generation of an analogical baroclinic motion. Contrariwise, if occasionally the baroclinic zonal flow has been excited, it evidently will compete with the barotropic flow and a significant baroclinic component of nearly-zonal jets can be expected. This result may reflect the fact that a zonal shear flow of a certain structure is stable with respect to small perturbations (Rhines, 1977; Kamenkovich et al., 1986).

3.4 Baroclinic meridional anisotropy

In the 1-layer computations, the energy transfer from zonal to meridional motion components is detected only in some particular cases and identified as the tendency towards energy equipartition between waves equal in length (i.e., towards spectral isotropy). No nonlocal (in the sense of wavelength) energy redistribution was observed (Reznik and Soomere, 1984a; 1984b). However, with the use of another closure a nonlocal directional energy transfer was noted, for example, in (Holloway and Hendershott, 1977).

A nonlocal energy exchange becomes evident in the later phase of several current experiments. Namely, a large-scale mostly meridional flow is generated starting from a certain time moment. This phenomenon appears explicitly only in the cases where also essential baroclinic zonal anisotropy is present, and becomes active after both zonal flow components have obtained a certain intensity (Figs. 11, 12).

Consider an example of the evolution of a wave system with an initially nearly absent zonal component of the barotropic mode (run 4; $F(\vec{\kappa},0) = p\kappa \exp(-\kappa^2)\cos^4\varphi$; $G(\vec{\kappa},0) = p\kappa \exp(-\kappa^2)$; $16p^{-1} = \pi^{3/2}(8 + 3\alpha)$). Differently from the above-discussed experiments, baroclinic energy now exceeds barotropic energy three times. Thus, baroclinic self-interactions will be relatively intense, at least during the initial phase of the experiment.

The evolution of the barotropic mode and its derivative, nevertheless, insignificantly differs from the above-described scenario (cf. Fig. 9). However, the baroclinic derivative field is greatly different from that in, e.g., run 1. At the outset it
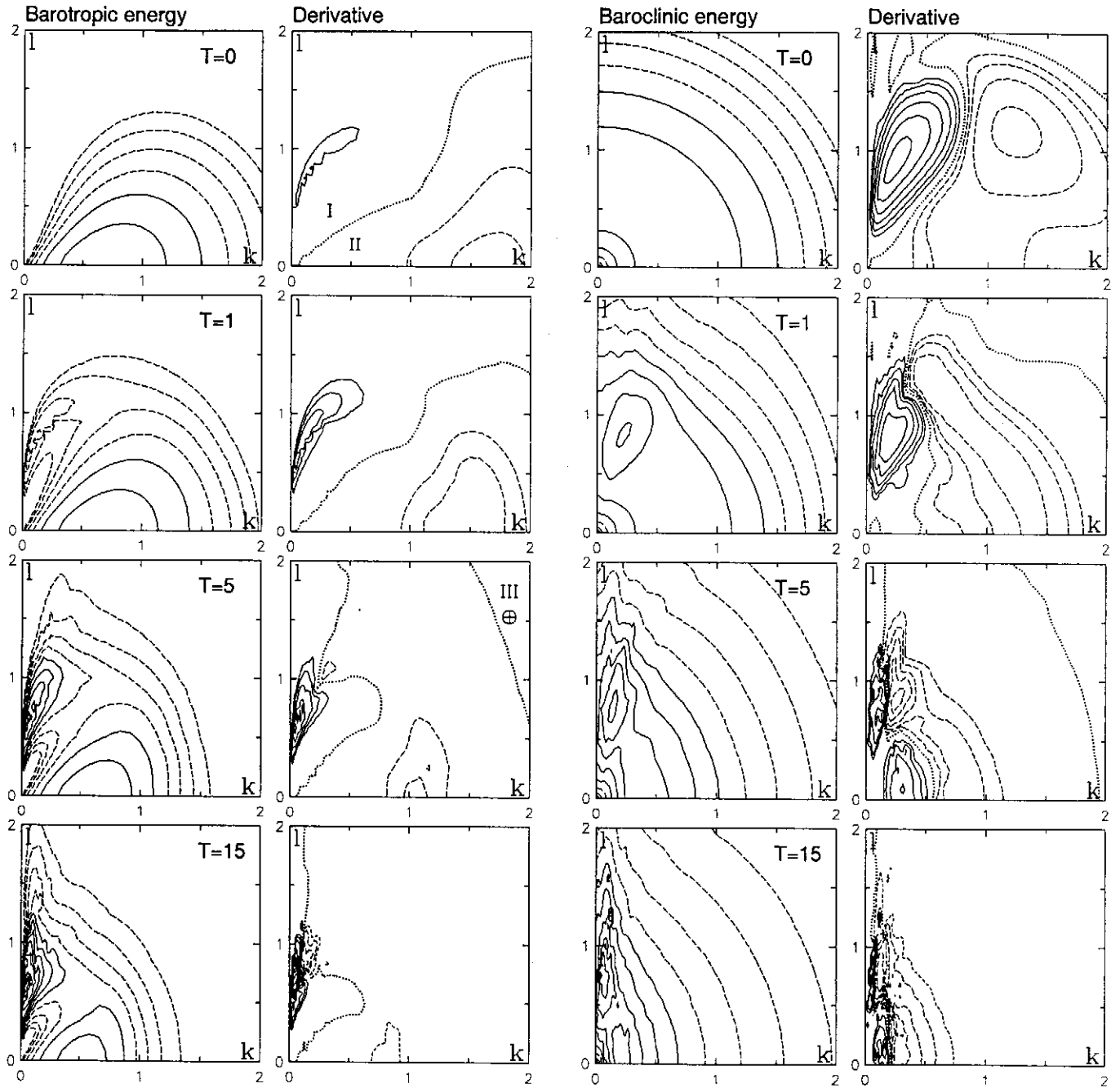
Fig. 11. As for Fig. 5, but for run 4 with initial functions $F(\vec{\kappa}, 0) = p\kappa \exp(-\kappa^2)\cos^4\varphi$; $G(\vec{\kappa}, 0) = p\kappa \exp(-\kappa^2)$; $16p^{-1} = \pi^{3/2}(8+3\alpha)$. An additional short-dotted contour at $\partial F/\partial T = -0.00562$ is plotted at $T = 15$.

contains inflow area I near the l-axis, outflow area II remote from this axis and two areas III of weak outflow. It more resembles the field of the barotropic derivative of run 1 (cf. Fig. 6). This predilection continues during most of the computational time: the $\partial G/\partial T$ field permanently retains an area of intensive inflow in the closest vicinity of the l-axis. Respectively, there arises a well-defined baroclinic zonal peak.

Further on, another maximum of $\partial G/\partial T$ close to the k-axis arises at $T \sim 2$, gains intensity fast, and remains comparable to the maximum near the l-axis. As a result, a relatively flattish spectral peak, a bit elongated in the l-direction, arises in the vicinity of the k-axis. It remains essentially lower than the zonal peak, but increases during all the later phase of the experiment. The peak is placed nearly completely closer to the origin than the zonal peak. Its maximum is located at $\vec{\kappa} \approx (0.3, 0.1)$. It corresponds to a mostly meridional flow with a horizontal scale approximately four times exceeding the scale of the initial motion. It is noteworthy that, differently from the zonal anisotropy, there is no significant frequency shift related with the generation of this peak.

The baroclinic meridional peak obviously arises owing to intermodal interactions. It is evidently unstable because baroclinic self-interactions should smooth it. However, this process apparently takes a long time, since the mean intensity of the interactions for $\kappa \approx 0.25$ is at least by two orders of magnitude less than at $\kappa \approx 1$.

4 Details of energy redistribution

4.1 Elementary interactions supporting the meridional anisotropy

The above has shown that an intensive energy inflow into the vicinity of the k-axis sets in only after both the modes have developed considerable zonal anisotropies. The observed zonal peaks often by more than one order exceed the mean energy level. Since the collision integrals are quadratic with respect to the spectra, the energy exchange rate of a certain wave vector $\vec{\kappa}^*$ may contain an extraordinarily large contribution if vectors $\vec{\kappa}_1^*, \vec{\kappa}_2^*$, resonantly interacting with $\vec{\kappa}^*$, both happen to lie near a zonal peak. Therefore, the energy flux to the meridional flow (i.e., to the baroclinic wave vectors $\vec{\kappa} \approx (\hat{k}, 0)$) may be related to interactions of nearly zonal harmonics.

The modes develop a zonal anisotropy, if any, at $\hat{k} \ll 1$, $\hat{l} \approx 1$. An arbitrary triad $\vec{\kappa}^* = (\hat{k}, 0)$, $\vec{\kappa}_1^* = (0, 1)$, $\vec{\kappa}_2^* = (-\hat{k}, -1)$ satisfies the resonance conditions provided the waves with $\vec{\kappa}^*, \vec{\kappa}_1^*$ represent the baroclinic and $\vec{\kappa}_2^*$ the barotropic mode (Fig. 13a). If $\hat{k} \approx 0.2$, both the vectors $\vec{\kappa}_1^*, \vec{\kappa}_2^*$ lie close to their modal maxima. The main contribution to $\partial G(\vec{\kappa}^*)/\partial T$ is roughly proportional to $G(\vec{\kappa}_1^*)F(\vec{\kappa}_2^*)$ and expresses an energy flow to $\vec{\kappa}^*$. This particular case demonstrates the possibility of supporting relatively large-scale meridional baroclinic disturbances at the expense of the barotropic nearly zonal flow. Obviously, this mechanism is active for other wave vectors $\vec{\kappa}, \vec{\kappa}_1, \vec{\kappa}_2 \approx \vec{\kappa}^*, \vec{\kappa}_1^*, \vec{\kappa}_2^*$ as long as

the described conditions are satisfied. There is no significant increase in energy for very long waves because the interaction coefficients of Rossby waves $C_{\vec{\kappa}_i, \vec{\kappa}_j}^{pmn}$ decrease as κ^4 if $\kappa \to 0$. The area of actual energy inflow is restricted to the values $\vec{\kappa}$, for which the interaction coefficients are big enough and there exist appropriate resonantly interacting waves with vectors positioned near to either spectral peak.

An analogous effect may occur in the case of self-interactions. However, the spectral maxima are usually too modest (baroclinic mode) or badly placed (barotropic mode) to activate such an energy transfer. The contribution including, say, the product $F(\vec{\kappa}_1^*)F(\vec{\kappa}_2^*)$ with both $\vec{\kappa}_1^*, \vec{\kappa}_2^*$ close to the barotropic maximum, remains small since this maximum is located extremly close to the l-axis and the vectors $\vec{\kappa}_1^*, \vec{\kappa}_2^*$ are nearly colinear. However, the energy removed from the barotropic zonal peak via the "erosion" process discussed above may be transformed a to mostly meridional flow and only then be isotropically redistributed. The energy inflow areas at $\kappa \leq 1$ remote from the l-axis in the later phases of some experiments (e.g., Fig. 6), may be related to this mechanism.

4.2 Interactions with baroclinic zonal flow

Let us consider interactions with the baroclinic zonal flow in mixed resonance triads. They involve vectors $\vec{\kappa} = (k, l)$, $\vec{\kappa}_1^\mp = (0, -l \mp l_d)$, $\vec{\kappa}_2^\pm = (-k, \pm l_d)$, where $l_d = (l^2 + a_1^2 - a_0^2)^{1/2}$ (Fig. 13b,c) and without any loss of generality we suppose $k, l \geq 0$. Since $\omega(\vec{\kappa}_1^\mp) = 0$, the frequencies of waves with $\vec{\kappa}, \vec{\kappa}_2^\pm$ are equal. The spectral symmetry yields $F(\vec{\kappa}_2^-) = F(\vec{\kappa}_2^+)$ and the contribution into $\partial G(\vec{\kappa})/\partial T$ is $[c_1 G(\vec{\kappa}_1^-) + c_2 G(\vec{\kappa}_1^+)][F(\vec{\kappa}_2^+) - \alpha G(\vec{\kappa})]$, where $c_1, c_2 \geq 0$ are proportional to $|\vec{\kappa}_1^\mp \times \vec{\kappa}_2^\pm|$.

Thus, the described interactions always try to decrease the difference $|F(k, l_d) - \alpha G(k, l)|$, hence creating an intermodal energy flux along the l-axis. The energy exchange takes place between harmonics of equal frequency [thus, Hasselmann's (1967) criterion is not violated] but of different wavelengths. For $k \ll 1$ this wavelength shift may result in energy exchange between motions of crucially different scales.

Basically, every perpetual tendency reveals a certain feature of the equilibrium state. In the case of barotropic Rossby waves an analogical mechanism (interaction between harmonics symmetric to the l-axis through the zonal flow) creates a tendency to spectral symmetrization (Reznik and Kozlov, 1981; Reznik and Soomere, 1984a). It is also active within the self-interaction of both the modes in the case in question. Its presence proves the impossibility of nonsymmetric equilibrium distributions.

Both interactions with the zonal flow occur between harmonics with equal frequencies and p-wavenumbers $\kappa^{(p)} = (k^2 + l^2 + a_p^2)^{1/2}$ (Jones, 1979). It is easy to see that, in the equilibrium state, the amplitudes of nonzonal harmonics with equal p-wavenumbers must be equal regardless of their relevance to the modes. Thus, intermodal interactions with the baroclinic zonal flow tend to adjust an appropriate balance of the modes. The above yields that interactions with the zonal flow tend to "copy" the spectral inhomogeneities between the modes, sim-
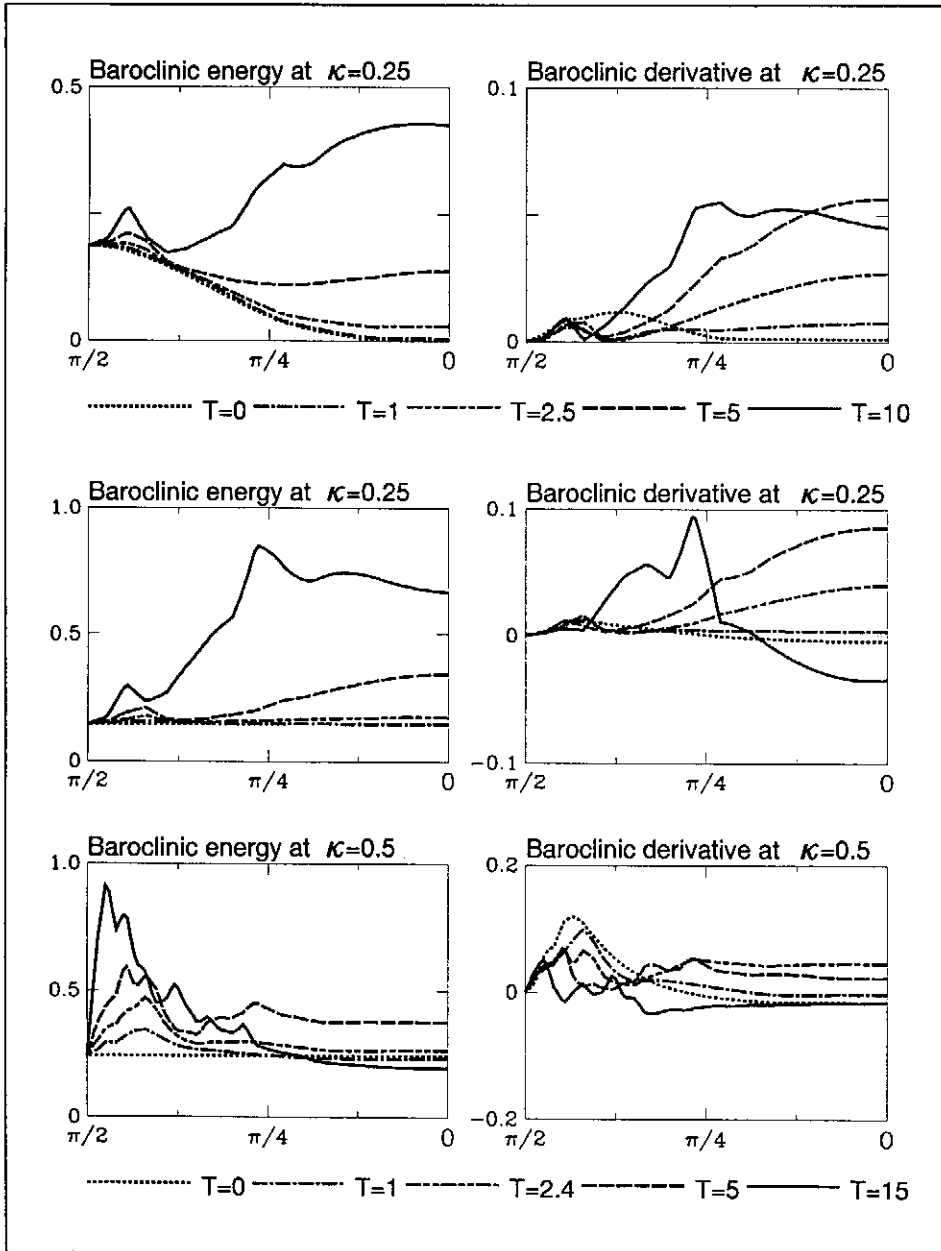
Fig. 12. Behaviour of the baroclinic energy spectrum (left) and its temporal derivative (right) at the curves $\kappa = $ const < 1. The results of run 6 (upper panels) and run 4 (middle and lower panels) are given. The meridional peak is mostly located at $\kappa \leq 0.25$ and tends to move closer to the origin.
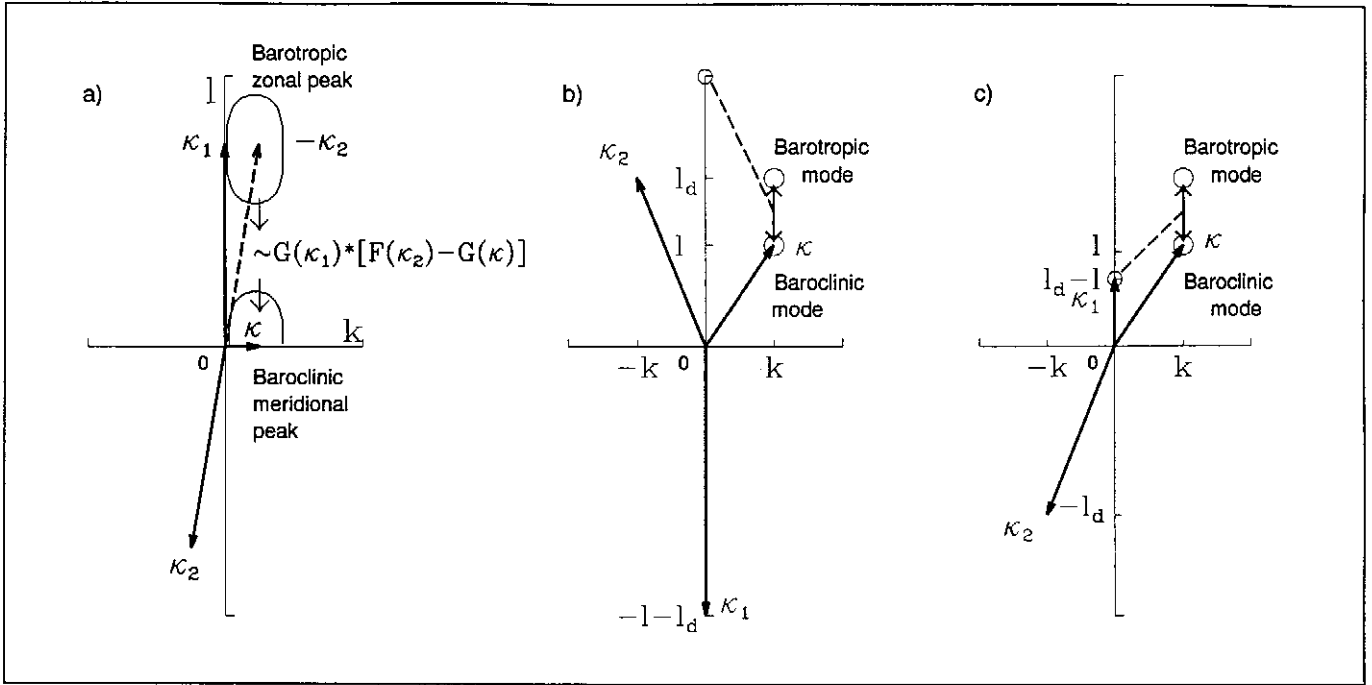
Fig. 13. Interactions with baroclinic zonal flow in mixed resonance triads. a) - interactions responsible for the generation of the baroclinic meridional anisotropy, b), c) - interactions creating intermodal energy flux, corresponding to the upper and lower signs in definitions of $\bar{\kappa}_1, \bar{\kappa}_2$, respectively. The intensity of these interactions is proportional to the amplitude of the baroclinic zonal flow with $\bar{\kappa}_1$. The interacting vectors are shown in the respective quadrants but the energy exchange coordinates in the first quadrant.

ultaneously "shifting" them by the distance $l_c = l_d - l$ alongside the l-axis. Energy conversion from the barotropic to the baroclinic mode causes a shift towards larger scales. Thus, barotropic peaks will be shifted towards the k-axis, whereby the inhomogeneities at $l < (a_1^2 - a_2^2)^{1/2}$ will be lost. Literally, the baroclinic meridional peak reflects only the "tail" of the barotropic zonal peak, farthest removed from the origin. Since the disposition of spectral peaks shows only a weak dependence on the nondimensional Rossby radii, the intensity of this mechanism may essentially depend on particular scaling.

Contrariwise, the inhomogeneities of the baroclinic spectrum will excite their smaller-scale barotropic "copies". With the current scaling, a barotropic zonal anisotropy may be anticipated at $l \approx 1.3$ with the baroclinic zonal peak arising simultaneously at $l \approx 0.7$. Indeed, a prolongation of the barotropic zonal peak at $l \approx 1.3$ in run 4 (Fig. 11) may be related with the mechanism discussed. However, this process may take a longer time because its intensity is proportional to the amplitude of the relatively long or short components of the baroclinic zonal flow $G(\bar{\kappa}_1^{\mp})$.

It should be noted that the cascade to higher modes owing to this mechanism results in enhancing mostly meridional motions. Contrariwise, an inverse process always increases the zonal anisotropy of the barotropic flow. As a fine conclusion, the generation of local spectral peaks within the modes finally results in an additional increase in the zonal anisotropy of the lower modes.

As compared to the pure barotropic case, the mechanism dis-

cussed above is a principally new phenomenon, created exclusively by the presence of the vertical structure of the motion. It is described by the collision integrals I_{110} and I_{011}, from the thermodynamical viewpoint responsible for creating the proper balance of the modes. A "catalyst" here, playing a central role in this process and amplifying it with its presence but itself remaining unchanged, is the baroclinic zonal flow. In contrast with the spectral symmetrization, the energy moves along the l-axis and may be redistributed between waves of drastically different lengths.

4.3 Entropy and interaction intensity

A fundamental property of Eqs. (2) and Eqs. (4) is that the system entropy necessarily increases with time [Eq. (8)]. Integral $H = \int \ln FG \, dk \, dl$ over $\mathbb{R}^2$ diverges for nonzero nontruncated equilibrated spectra F_{eq}, G_{eq}. The absence of a mean flow results in another singularity at the origin. [Eqs. (2) are derived using this restriction; otherwise the kinetic equation would have an essentially different form (Benney and Newell, 1967)]. The former inconvenience is removed by the truncation introduced in Section 2.4. It is convenient to remove the latter by using an arbitrary bilateral truncation $0 < \delta < \kappa < 4$, where δ is smaller than the grid step.

A well-known result states that $\partial F_p / \partial T \geq 0$ at points where $F_p = 0$. Thus, in the course of time ordinarily both the spectra will obtain positive values. An exception is constituted by singular spectra; e.g., stationary spectra concentrated on a circle $\kappa = $ const or on a line $cl + bk = 0$ (Soomere, 1987). At the l-axis always $\partial F_p / \partial T \equiv 0$, reflecting the fact that
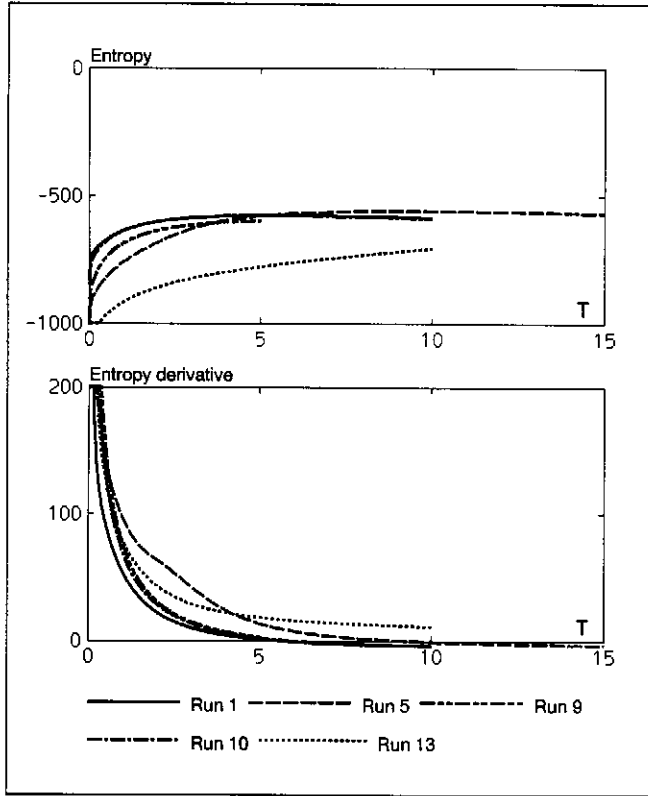
Fig. 14. Temporal behaviour of entropy (upper panel) and its derivative (lower panel). Notations are the same as for Fig. 3.

Rossby-wave resonant interactions do not alter the zonal flow. The absence of the latter is, however, hardly possible in realistic situations. On the one hand, it can easily be avoided by assigning to F_p a small positive value at each node. If small enough, its effect is evidently negligible. On the other hand, we are mostly interested in the entropy *variation* and its actual value in the narrow vicinity of the l-axis may be neglected. Thus, we exclude the points with $FG = 0$ when computing the entropy and its derivative (in runs $2,4\ldots6,8,10\ldots12$ during all the simulations, in runs $3,7,9,13\ldots15$ only at $T = 0$).

The entropy increasing law was found to hold in all the experiments conducted. The entropy derivative is initially of the order of $10^3\ldots10^5$, but decreases fast and monotonously with time (Fig. 14). To the very end of some runs it reaches small negative values evidently owing to computational inaccuracy. The initial fast entropy alteration results from both the weakness of shorter waves and the absence of a motion component (runs $2\ldots8,11\ldots12,14\ldots16$).

The total entropy increases roughly twice during our experiments and usually remains nearly unchanged in their final phases (Fig. 14). Only in runs $10\ldots12$ does the entropy grow up to the end of the simulations, evidently owing to the inactivity of the generation of baroclinic motions. The manner of the temporal entropy alteration suggests that computed final states are close to equilibrium ones. The entropy of isotropic equilibrium states for runs $1\ldots9$ is roughly -550 (Appendix A). Its good concordance with the simulated values
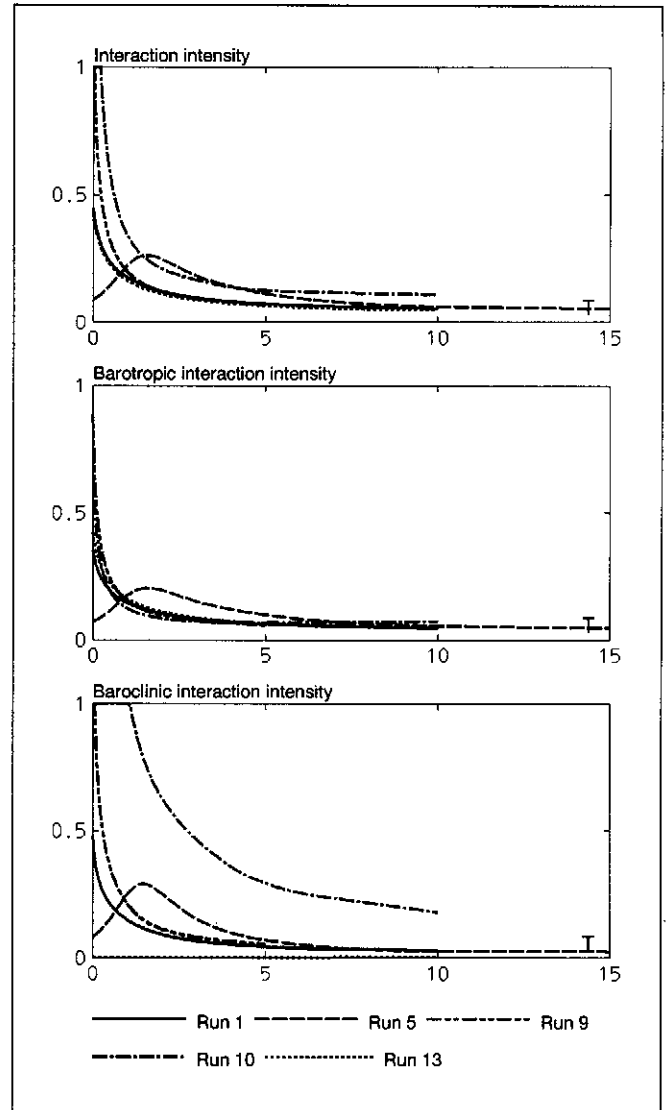

Fig. 15. Temporal behaviour of the integral intensity of interactions I (uppermost panel), its barotropic (middle panel) and baroclinic (lower panel) components. Notations are the same as for Fig. 3.

apparently shows that zonal peaks do not play any important role in entropy alteration.

Another important measure of the processes in question is the integral intensity of interactions

$$I = I_0 + I_1 = \int \left(|\partial F/\partial T| + \alpha|\partial G/\partial T| \right) dk\, dl. \qquad (16)$$

It vanishes for an arbitrary stationary state and apparently is small for the spectra close to them. It may behave nonmonotonously, as noted in several runs. However, a temporary increase in I or its components takes place only in initial phases of runs 5, 11 and 14 and is evidently connected with the low initial level of the zonal component of the motion. Since the latter serves as a "catalyst" of resonant interactions, the interaction intensity may increase to some extent as it enhances. The values of I, I_0 and I_1 fall off monotonously, beginning from a certain time moment (Fig. 15). The details of this fall-
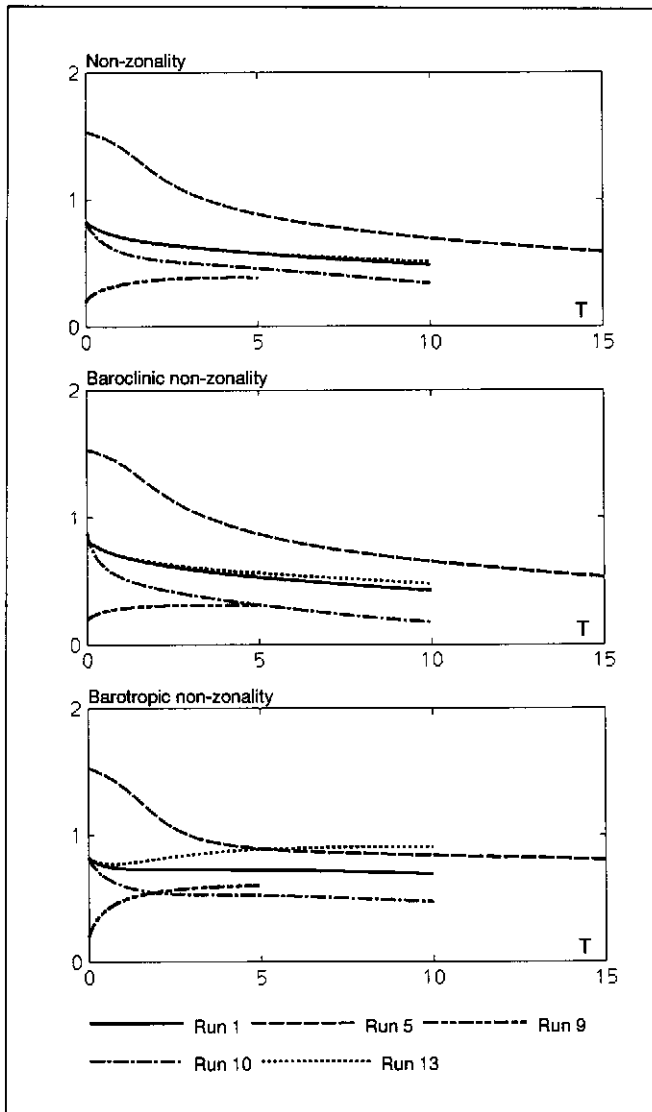
Fig. 16. Temporal behaviour of the non-zonality index B_{NZ} (uppermost panel), its barotropic (middle panel) and baroclinic (lower panel) components. Notations are the same as for Fig. 3.

off essentially depend on the initial conditions, but typically it takes place quite rapidly. During the computational time, I usually decreases more than 10 times as compared to its value at $T = 0$ (Table B1). In the few runs with nonmonotonous behaviour of I, it falls by a factor of $3\ldots4$ as compared to its maximum value. As noted in section 3.2, the intensity of interactions for the baroclinic mode usually decreases faster than that of the barotropic mode.

4.4 Balance between motion components

Although the zonal peaks are extremly high, they are also concentrated within a relatively small area of wave vectors. The balance between the zonal and the isotropic motion components may be characterized by the "non-zonality" index

$$B_{NZ} = B_{NZ0} + \alpha B_{NZ1} =$$

$$= \int (\varphi - \pi/2)^2 F\,dk\,dl + \alpha \int (\varphi - \pi/2)^2 G\,dk\,dl,$$

which vanishes if the wave system decays into a zonal motion. Typically, B_{NZ} decreases to some extent (and increases only in a few simulations with a considerable initial zonal anisotropy), confirming an average intensification of the zonal component of the motion (Fig. 16). The quantity B_{NZ0} ordinarily decreases, while B_{NZ1} (which increases in some experiments) becomes nearly constant at $T \geq T_{\max}/3$. This also confirms that the barotropic flow intensively gains zonal anisotropy while the baroclinic mode reveals no directional preference.

Nevertheless, no essential decay of any of these measures is observed. All of them rather have a nonzero limit; thus, the ultimate decay of the wave system (or one of its modes) into a zonal flow is unlikely.

An interesting detail is the energy balance between the modes. Rhines (1977) suggested that barotropization occurs fast owing to phase locking between coherent structures in adjacent layers. A similar conclusion has been reached by Salmon (1980). Within isolated triads energy is more likely to move into the lowest mode. Barotropization of the synoptic motions was detected during the final stage of the "POLYMODE" experiment (e.g., Kamenkovich et al., 1986). In numerical experiments, ordinarily a system of barotropic zonal jets arises.

Still, the full barotropization of the flow in all cases is unlikely (Rhines, 1977). It is inhibited in both the equilibrium statistical mechanics and the classical weakly nonlinear theory (Holloway, 1986; Kozlov et al., 1987). Also, the treatment given above has demonstrated no decay of the baroclinic energy. Nevertheless, the full barotropization of the weakly nonlinear flows through exciting a total barotropic zonal flow cannot be excluded.

The modal structure of classical equilibrium states is uniquely defined by the initial energy and enstrophy (Appendix A). For the actual final states, the ratio of the modal energies E_1/E_0 also depends on the energy and enstrophy fluxes into the zonal flow. Since details of these fluxes are unclear even for the 1-layer case, to a first approximation, we shall neglect them.

The initial ratio E_1/E_0 for runs $1\ldots9$ varies from $1/3$ to 3. Its equilibrium value depends on the truncation radius and the ratio Y/E of the total enstrophy to energy (see Appendix A). The latter equals $(3 + 5\alpha)/(2 + 2\alpha) = 5/3$ for initial states with energy equipartition between the modes (runs $1, 5, 6, 8$ and 9), or $(24 + 15\alpha)/(16 + 6\alpha) \approx 1.57$ for the runs with initially dominating barotropic or $(9 + 40\alpha)/(3 + 8\alpha) \approx 1.85$ for the initially dominating baroclinic mode. These values, as well as the equilibrium ratio E_1/E_0 (it equals to 0.259, 0.243 or 0.289, respectively), vary insignificantly. Therefore, at $T = 0$ this ratio typically (except for runs 2, 3 exceeds the equilibrium one) several times.

Figure 17 shows the behaviour of the modal energies. Quite surprisingly, in several runs baroclinic energy increases additionally and starts to decrease only in their final phases. In
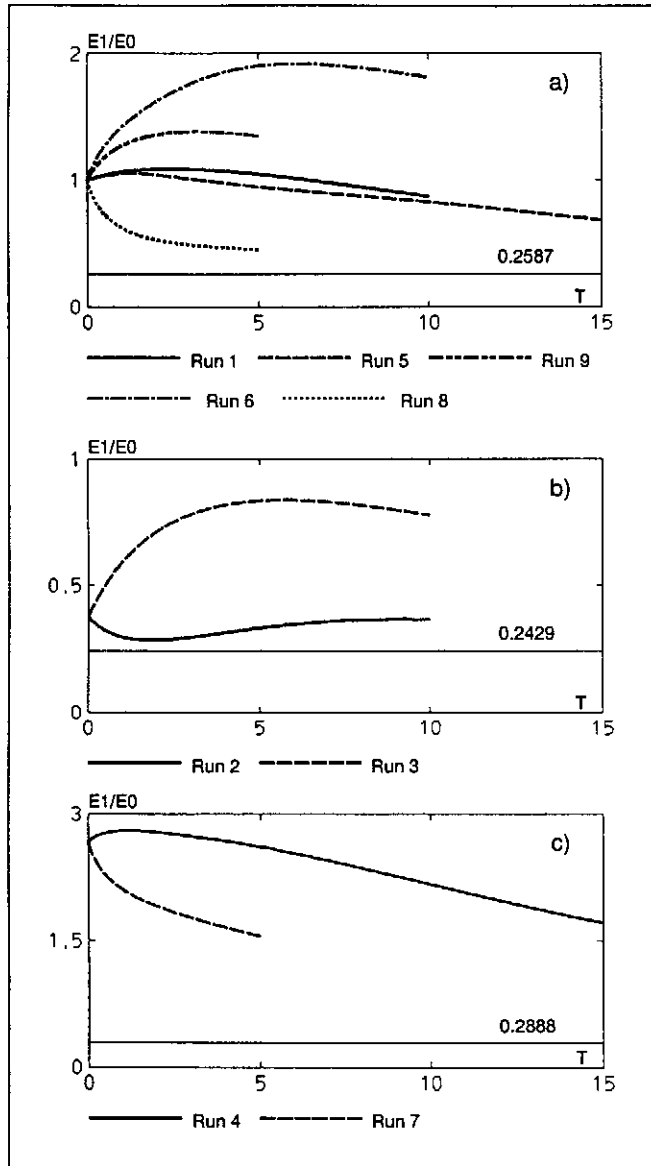
190

Fig. 17. Evolution of the modal structure of motions: a) - runs with initial energy equipartition between modes, b) - runs with initially mostly barotropic motions and c) - runs with mostly baroclinic initial flow.

some runs, the energy transfer rate into the barotropic mode is nearly constant until the end of the simulations, which suggests that the computed final ratio E_1/E_0 is quite far from that of the equilibrium state.

The fact that the baroclinic energy permanently exceeds its predicted level suggests that the energy and enstrophy fluxes into the zonal flow are unmatched. Fig. 17 shows that the equilibrium ratio E_1/E_0 increases with the increase in Y/E. Therefore, the energy flux into the zonal flow apparently exceeds that of the enstrophy flux. This is possible only if energy cascades into either smaller wavenumbers of the zonal flow or into the lower modes. Since energy typically flows to the baroclinic mode (Fig. 17), the generation of zonal peaks apparently enhances the scale-increasing process.

It should be noted that barotropization of both simulated and

realistic synoptic motions does not contradict the features described. They only indicate that it may occur highly selectively and its intensity depends on the initial state. We have seen that it is always active for the zonal part of the motion, but may have an essentially weaker effect on other flow components.

5 Discussion and concluding remarks

The main evolution scenario of weak geostrophic turbulence consists in the generation of a fully barotropic nearly zonal flow accompanied by damping of the baroclinic zonal anisotropy. Another (less frequent) scenario consists in the generation of a multi-modal zonal flow. However, the mutual relationship of these scenarios as well as their concordance with the evolution towards an equilibrium state still remains unclear.

As a basically new phenomenon, large-scale mostly meridional baroclinic motions may be excited owing to interactions between nearly zonal flow components. It arises from the interplay of the β-effect, the nonlinearity and the vertical structure of the flow. A principal point is that these baroclinic motions may gather energy from the barotropic nearly zonal flow while all the other processes seem to support it.

The phenomena of reinforcement of the zonal component and the barotropization of large-scale geophysical flows are both widely known. An interesting peculiarity of the described spectral evolution consists in the highly selective joint influence of these effects. It ordinarily supports the barotropic flow components relatively short in wavelength at the expense of baroclinic harmonics. Also, mixed-triad interactions usually tend to amplify the barotropic zonal flow; thus, the energy flux into the lower modes results in an additional enhancement of the zonal component of motion.

Several of the features discussed do not coincide with the classical concept of final energy equipartition between all the waves. First, the incessant generation of anisotropy for the system evolving towards a thermal equilibrium. However, for the particular case of (specifically anisotropic) geophysical dynamics the appearance of ordered flows possessing the entropy maximum has become traditional (Holloway, 1986, among others). Second, the dependence of the modal structure of the equilibrium zonal flow on the initial conditions. It might be explained in the same way as the equilibrium "temperatures" depend on the initial energy and entropy. The third parameter of the (generalized) equilibrium distributions may arise from the singular conservation law (7c). Third, the fact that there arises an additional (mostly meridional) spectral maximum is deeply nontrivial. Even its provisional generation reflects a specific self-organization process, activated by the vertical structure of the motion. In multi-layer models, multiple peaks may be generated in the spectra of the modes. Although the 2-layer model poorly represents the dynamics of the Earth's atmosphere and the oceans, the latter feature suggests that frequent evidence of large structures with a considerable meridional component of the flow (e.g., blocking events) may be a built-in feature of stratified geophysical

flows. The fact that the meridional peak becomes evident only after the excitation of a multi-modal zonal flow may be useful in predicting these phenomena.

The intensive energy transfer into extremely low-frequency nearly zonal motions may, in principle, indicate that spectra of free Rossby wave systems evolve only to a certain degree and then "freeze". Once generated, barotropic zonal motions may be regarded as practically insensitive to weakly nonlinear interactions since the time scale for their changes may considerably exceed the time of their generation. Also, after they have gathered a certain amplitude, assumptions of the kinetic approach may not hold. Such a "frozen" state would have nothing in common with thermodynamics and probably would represent a stationary solution to the kinetic equation. Nevertheless, several facts show that the zonal flow plays important roles in weak geostrophic turbulence. It serves as a "catalyst" of spectral changes towards an equilibrium. The interplay of its components leads to the excitation of the baroclinic meridional anisotropy. Incessant "copying" of zonal spectral peaks takes place between the modes. These features suggest that such simple "freezening" is unlikely.

here is a great deal evidence to show that the computed final spectra are close to the (at least local) equilibrium. Namely, the immense decrease in the entropy alteration rate, the drastic decay of the interaction intensity and the isotropization of nonzonal spectral components are weighty arguments proving that spectral components match a Raleygh-Jeans distribution. Analysis of the modal structure, however, shows that the total spectrum is still far from its final state. The evolution process can be interpreted as multi-staged adaptation towards an equilibrium, similar to that in (Errico, 1984). As the first step, the nonzonal parts of both spectral components take a form close to a "local" thermodynamical equilibrium $F_i = (a_i + b_i \kappa^2)^{-1}$, with "temperatures" a_i, b_i not necessarily overlapping. The second step consists in a more gradual adjustment of the "temperatures".

The presence of spectral peaks may break the latter into substages. A "copy" of the barotropic zonal peak emerges as the baroclinic meridional peak. Later on, it will evidently be smoothed owing to baroclinic self-interactions. The characteristic time of the latter process probably exceeds the duration of the earlier stages by several orders of magnitude.

This concept suggests an in itself interesting cascade-like approach to the final state, with alternating generation of a medium-scale zonal flow, then a system of large-scale mostly meridional motions and, at the very end, a new phase of extremely slowly-changing motion components. This peculiarity may be one of the reasons why direct simulations of the 2-layer β-plane turbulence need an enormous time interval for zonal components to become statistically steady (Vallis and Maltrud, 1993).

Realistic synoptic-scale motions evidently have a spectrally wide "background" of weak Rossby waves. It should also be implicitly present in high-resolution numerical models of oceans and/or the atmosphere. The current study describes a part of the background evolution, which happens owing to the weakly nonlinear interactions. The interactions of the "back-ground" with strongly nonlinear structures as well as the effects related to wave generation and decaying processes additionally affect its evolution. Nevertheless, the principal effects described above are always present. Owing to their "eternal" nature, their joint effect can apparently be detected. The extreme sharpness of computed zonal peaks suggests that the flows generated as a result of weakly nonlinear interactions may compete with quasi-stationary currents.

Appendix A   Calculation of equilibrium "temperatures"

Physically, there must exist a one-to-one relationship between the values of constraints E, Y [Eqs. (5,6)] and the equilibrium "temperatures" a, b. From the mathematical viewpoint, this declaration needs a rigorous proof. Let $c = a/b$; the conservation laws then read

$$\ln \frac{c+16}{c} + \alpha \ln \frac{c+17}{c+1} = \frac{Eb}{\pi}, \tag{A1}$$

$$16(\alpha + 1) - c \ln \frac{c+16}{c} - \alpha c \ln \frac{c+17}{c+1} = \frac{Yb}{\pi}. \tag{A2}$$

Eqs. (A1) are derived for the truncation $\kappa \leq 4$ and the set of Rossby numbers $a_0 = 0$; $a_1 = 1$. Their generalization for other values of these parameters is straightforward. From Eqs. (A1) it follows that

$$aE + bY = 16\pi(\alpha + 1), \tag{A3}$$

an elementary result warning that the initial energy and enstrophy cannot be chosen arbitrarily. With the help of Eq. (A2), Eq. (A1) is reduced to

$$\begin{aligned} f(c) &= \ln(c+16) - \ln c + \alpha \ln(c+17) \\ &\quad - \alpha \ln(c+1) - 16(\alpha+1)(c+g)^{-1} = 0, \end{aligned} \tag{A4}$$

where $g = Y/E$. Eq. (A4) demonstrates that the ratio of the equilibrium "temperatures" only depends on the ratio of the enstrophy and the energy. From the general features of logarithmic and rational functions it can be understood that Eq. (A4) has, if any, a unique positive solution $c(\alpha, g)$.

Since $f(0) = \infty$ and $f(\infty) = 0$, Eq. (A4) has a positive zero only provided the function $f(c)$ has a minimum $f(\hat{c}) \leq 0$, where $0 < \hat{c} < \infty$. The derivative $f'(c)$ is a rational function and the equation $f'(c) = 0$ is reduced to

$$d_3 c^3 + d_2 c^2 + d_1 c + d_0 = 0, \tag{A5}$$

where

$$\begin{aligned} d_3 &= -2g + 16 + 2s, \\ d_2 &= -g^2 - 36g + 4sg + 288 + 17s, \\ d_1 &= -18g^2 + sg^2 - 34g + 34sg + 272, \\ d_0 &= -17g^2 + 17sg^2 \end{aligned} \tag{A6}$$
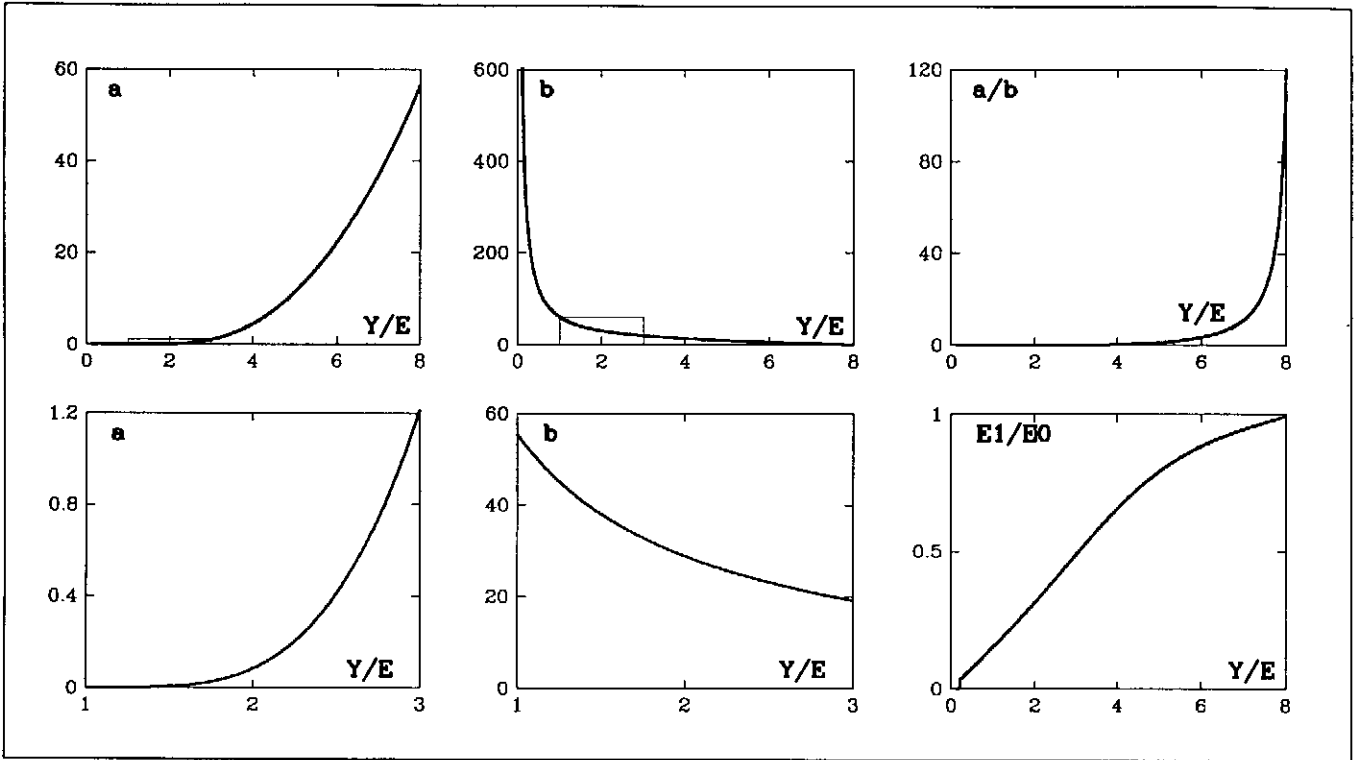
Fig. 18. Dependence of the equilibrium "temperatures" a (left column) and b (middle column) on the ratio of initial energy to enstrophy. Right column shows the analogical dependence of $c = a/b$ and the ratio E_1/E_0 of the baroclinic and the barotropic energy in the equilibrium state.

and $s = \alpha/(\alpha + 1)$. Obviously, $d_0 \leq 0$ provided $\alpha > 0$. Further, the coefficients $d_i(g = 0, \alpha) > 0, i = 1, 2, 3$, tend to negative infinity as $g \to \infty$ and have exactly one zero $g_i > 0$. It is easy to see that $3 < g_1 < 4, 5 < g_2 < 6$ and $g_3 = 8 + \alpha/(\alpha + 1)$. From the mutual location of the points g_i it follows that the function $f'(c)$ has exactly one zero $0 < \hat{c} < \infty$ provided

$$g < g_{max} = 8 + \alpha/(\alpha + 1). \tag{A7}$$

If g is of greater value, Eq. (A4) has no positive solutions. This condition limits the set of physically realizable values of energy and enstrophy. For pure barotropic motions it reads $g < 8$. Thus, stratified flows offer more freedom in choosing their initial states.

If (A4) is satisfied, the derivative $f'(c) < 0; c < \hat{c}$ and $f'(c) > 0; c > \hat{c}$. Since $f'(0) = -\infty; f'(\infty) = 0$, the function $f(c)$ decreases if $0 < c < \hat{c}$, has one extremum $f(\hat{c}) < 0$ and increases for $c > \hat{c}$, asymptotically reaching zero from the negative side. Therefore, Eq. (A3) has exactly one solution $c^* \in (0, \hat{c})$.

Figure A1 shows the behaviour of the quantity $c = c(g)$ as well as of the equilibrium "temperatures". The value of c vanishes at $g = 0$, is quite small in all the cases considered in this study (typically of the order of a few thousandths), but increases extremly fast starting from $g \approx 6$, and tends to infinity as $g \to 8 + s$. Both the equilibrium "temperatures" reveal quite versatile behaviour in their domains. At $g = 0$ the "temperature" b has an infinite value, while a vanishes. The

corresponding spectrum is formally devoid of enstrophy, singular and concentrated at the origin. As g increases, a also increases while b decreases. At the limit $g \to 8 + s$ we have $b \to 0$ and $a \to \infty$. This limit, however, leads to a controversy and the corresponding spectrum cannot be constructed. The reason is that Eq. (A7) serves as a condition ensuring the existence of an *extremum* of $f(c)$. In order to reach its zero value the parameter g must be strictly less than its limiting value g_{max}. Differently from the "temperatures", the equilibrium ratio of baroclinic to barotropic energy reveals a nearly linear dependance on g, with a somewhat weaker increase for $g > 5$. For most of the performed experiments, the equilibrium "temperatures" $a \sim 0.01; b \sim 40$.

For the equilibrium entropy with "temperatures" a, b, we have:

$$
\begin{aligned}
H/\pi &= 32(1 - \ln b) + c \ln c + (c + 1)\ln(c + 1) \\
&\quad -(c + 16)\ln(c + 16) - (c + 17)\ln(c + 17).
\end{aligned}
$$

The equilibrium values of the entropy for runs $1 \ldots 9$ differ insignificantly and are close to -550 (Table B1).

Appendix B Parameters of numerical simulations.

The main parameters of experiments are listed. Simulations are classified (**type of run**) as follows. Basic runs $(1 \ldots 9)$ - with initial conditions resembling those of the pure barotropic simulations (Reznik and Soomere, 1984a), mode generation -

Table B1. Parameters of numerical experiments

No.	Type of run	Initial spectra	Time steps	T_{max}	$\Delta T_{t=0}$	ΔT_{mean}	∂E/∂T(%) T=0	max	T_{max}	∂Y/∂T(%) T=0	max	T_{max}	Y/E	a	b	H	T=0	min	max/min
1	Basic runs	1,1	520	10	0.025	0.019	0.31	0.65	10	1.66	-3.32	8.4	1.67	0.0102	36.2	-551	0.45	0.053	8.4
2		1,2	700	10	0.025	0.014	0.18	0.68	10	1.36	-2.75	9.5					0.48	0.051	9.4
3		1,3	700	10	0.025	0.014	0.38	0.59	10	1.67	-2.74	9.2	1.57	0.0052	38.4	-557	0.48	0.05	9.5
4		2,1	900	15	0.025	0.017	0.10	0.76	15	1.05	-2.63	12	1.85	0.0284	32.6	-541	0.28	0.06	4.7
5		2,2	550	15	0.1	0.027	-0.04	0.35	4	-0.04	-3.26	13					0.09	0.053	4.9
6		2,3	600	10	0.025	0.017	-0.12	0.62	3.5	-0.78	1.04	1.2	1.67	0.0102	36.2	-551	0.33	0.061	5.4
7		3,1	700	5	0.01	0.007	0.54	0.80	0.5	2.96	3.03	1.5	1.85	0.0284	32.6	-541	1.02	0.079	12.9
8		3,2	700	5	0.01	0.007	-0.01	0.75	5	1.89	2.39	0.3					1.32	0.070	18.8
9		3,3	700	5	0.01	0.007	0.89	1.05	0.3	2.66	3.29	0.3	1.67	0.0102	36.2	-551	1.20	0.068	17.6
10	Mode generation	6,1	1350	10	0.01	0.0074	0.32	1.31	1.4	5.7	-7.59	7.1					2.27	0.108	21.0
11		6,2	1450	10	0.01	0.0069	-0.29	3.89	10	-0.29	-9.17	6.1	2.5	0.3251	24.0	-510	0.32	0.11	8.5
12		6,3	1800	5	0.005	0.0028	1.21	2.88	0.7	10.20	12.89	0.3					3.85	0.115	33.5
13		1,6	700	10	0.025	0.014	0.26	1.0	10	1.43	-1.55	8.5					0.42	0.049	8.6
14		2,6	700	10	0.025	0.014	-0.04	0.42	4.5	-0.04	-1.64	10	1.5	0.0031	40.2	-562	0.09	0.068	3.7
15		3,6	950	10	0.0125	0.0105	0.34	1.57	10	1.65	2.8	0.5					1.14	0.047	24.3
16	Dependance on α	α = 0.05	280	5	0.025	0.018	0.28	0.45	1.2	1.53	-2.67	5	1.55	0.0122	34.1	-545	0.44	0.072	6.1
17		α = 1	700	10	0.025	0.014	0.14	1.11	10	1.33	1.65	0.6	2.0	0.0015	50.3	-584	0.39	0.061	6.3
18		α = 5	1500	10	0.01	0.0067	0.34	1.05	1.2	4.5	-6.87	6.8	2.33	$0.0^8 4$	29.3	-678	1.57	0.091	17.3
19	Shifted maximum	7,7	2000	10	0.05	0.005	0.41	1.19	10	2.37	5.34	6.9	2.04	0.0707	29.5	-530	0.70	0.065	10.8
20		8,8	1700	10	0.01	0.0058	0.44	2.21	10	3.06	-8.7	5.3	2.5	0.331	23.9	-510	1.03	0.078	13.2
21		9,9	1200	15	0.025	0.0125	0.07	0.27	4.7	0.55	0.77	2.6	0.92	$0.0^5 15$	65.8	-611	0.16	0.03	5.2

with a purely baroclinic (10...12) or with a practically barotropic initial flow (13...15), dependance on α - run 1 with isotropic initial conditions is repeated with various values of the ratio of the layers' thicknesses, shifted maximum - experiments on isotropic initial spectra with their maxima at different wavelengths.

The shapes of the **initial spectra** are coded as follows:

(1) $\kappa \exp(-\kappa^2)$ (isotropic);

(2) $\kappa \exp(-\kappa^2) \cos^4 \varphi$ (mostly meridional motions);

(3) $\kappa \exp(-\kappa^2) \cos^4 \varphi$ (mostly zonal motions);

(6) $F \equiv 0$ for barotropic mode; $G = 0.001\kappa \exp(-\kappa^2)$ for baroclinic mode;

(7) $\kappa \exp(-2\kappa^2)$ (isotropic; with maximum at $\kappa = 0.5$);

(8) $\kappa \exp(-\kappa^3/3)$ (isotropic with maximum at $\kappa = 1$);

(9) $\kappa \exp(-\kappa^4/10)$ (isotropic with maximum at $\kappa \approx 1.25$).

The first number in this column indicates the initial shape of the barotropic mode, the second index that of the baroclinic mode. The spectra are normalized to $E = 1$ at $T = 0$.

Further, number of **time steps** performed, time moment by which a simulation was ended (T_{max}); the initial ($\Delta T_{t=0}$) and the mean (ΔT_{mean}) values of the time step are given. The relative alteration of the total energy ($\partial E/\partial T$) and the total enstrophy ($\partial Y/\partial T$) are given in percentages at $T = 0$, also their maximum values are presented (**max**) together with the time moment at which the maxima are reached. Next, the characteristics of the isotropic equilibrium distributions corresponding to the ratio of initial enstrophy and energy (Y/E),

equilibrium "temperatures" (a, b) and the equilibrium value of entropy are printed. For the total **interaction intensity** (Eq. 17), its initial ($T = 0$) and minimum (min) values are given together with the total decrease in this parameter (max/min). This measure behaves nonmonotoneously only in runs No. 5 (maximum value $I_{max} = 0.26$ is achieved at $T = 1.5$), No. 11 ($I_{max} = 0.93$ at $T = 0.7$) and No. 14 ($I_{max} = 0.25$ at $T = 1.5$).

References

Balk, A. M., Zakharov, V. E., and Nazarenko, S. M., On non-local turbulence of the drift waves, *Soviet Phys., JETP, 71*, 249–260, 1990.

Bartello, P. and Holloway, G., Passive scalar transport in β-plane turbulence, *J.Fluid Mech., 223*, 521–536, 1991.

Benney, D. J. and Newell, A. C., Sequential time closures for interacting random waves, *J. Math. Phys., 46*, 363–393, 1967.

Benney, D. J. and Newell, A. C., Random wave closures, *Stud. Appl. Math., 48*, 29–53, 1969.

Carnevale, G. F., Statistical features of the evolution of two-dimensional turbulence, *J. Fluid Mech., 122*, 143–153, 1982.

Carnevale, G. F. and Martin, P. C., Field theoretical techniques in statistical fluid dynamics: with application to nonlinear wave dynamics, *Geophys. Astrophys. Fluid Dynamics, 20,* 131–164, 1982.

Carnevale, G. F., Salmon, R., and Frisch, U., *h*-theorems in statistical fluid mechanics, *J. Phys. A, 14,* 1701–1718, 1981.

Charney, J. G., Geostrophic turbulence, *J. Atm. Sci., 28,* 1087–1095, 1971.

Errico, R., The statistical equilibrium solution of a primitive-equation model, *Tellus, 36A,* 42–51, 1984.

Hasegawa, A., Maclennan, C. C., and Kodama, Y., Nonlinear behaviour and turbulence spectra of drift waves and Rossby waves, *Phys. Fluids, 22,* 2122–2129, 1979.

Hasselmann, K., On the nonlinear energy transfer in a gravity-wave spectrum. Part 1. General theory, *J. Fluid Mech., 12,* 481–500, 1962.

Hasselmann, K., A criterion for nonlinear wave stability, *J. Fluid Mech., 30,* 737–739, 1967.

Hasselmann, S. and Hasselmann, K., *A symmetrical method of computing the nonlinear transfer in a gravity wave spectrum,* vol. A52 of *Hamburger Geophysikalische Einzelschriften,* Universität Hamburg, Hamburg, 1980.

Hasselmann, S. and Hasselmann, K., Computations and parametrizations of the nonlinear energy transfer in a gravity-wave spectrum. Part I: A new method for efficient computations of the exact nonlinear transfer integral, *J. Phys. Oceanogr., 15,* 1369–1377, 1985.

Hasselmann, S., Hasselmann, K., Allender, J. H., and Barnett, T. P., Computations and parametrizations of the nonlinear energy transfer in a gravity-wave spectrum. Part II: Parametrizations of the nonlinear energy transfer for application in wave models, *J. Phys. Oceanogr., 15,* 1378–1391, 1985.

Holloway, G., Eddies, waves, circulation and mixing: Statistical geofluid mechanics, *Ann. Rev. Fluid Mech., 18,* 91–147, 1986.

Holloway, G. and Hendershott, M., Stochastic closure for nonlinear Rossby waves, *J. Fluid Mech., 82,* 747–765, 1977.

Jones, S., Rossby wave interactions and instabilities in a rotating, two-layer fluid on a beta-plane. Part 1: Resonant interactions, *Geophys. Astrophys. Fluid Dynamics, 11,* 289–322, 1979.

Kamenkovich, V. M., *Fundamentals of ocean dynamics,* vol. 16 of *Elsevier Oceanographic Series,* Elsevier, Amsterdam, 1977.

Kamenkovich, V. M. and Reznik, G. M., Rossby waves, in *Physics of the ocean,* vol. 1: Hydrophysics, pp. 300–358, Nauka, Moscow, 1978.

Kamenkovich, V. M., Koschlyakov, V. N., and Monin, A. S., *Synoptic eddies in the ocean,* D.Reidel Publishing Company, Dordrecht, Holland, 1986.

Komen, G. J., Cavalieri, L., Donelan, M., Hasselmann, K., Hasselmann, S., and Janssen, P. A. E. M., *Dynamics and modelling of ocean waves,* University Press, Cambridge, 1994.

Kozlov, O. V., Reznik, G. M., and Soomere, T., Weak turbulence on the β-plane in a two-layer ocean, *Izvestiya, USSR Academy of Sci., Atmospheric and Oceanic Physics, 23,* 869–874, 1987.

Kraichnan, R. H. and Montgomery, D., Two-dimensional turbulence, *Repts. Progr. Phys., 43,* 548–619, 1980.

Lee, S. and Held, I., Baroclinic wave packets in models and observations, *J. Atm. Sci., 50,* 1413–1428, 1993.

Longuet-Higgins, M. S. and Gill, A. E., Resonant interactions between planetary waves, *Phil. Trans. Roy. Soc. Lond., 294,* 120–140, 1967.

Marshall, H. G., A note on the direction of energy movement in wavenumber of a two-layer model, *Dyn. Atm. Oceans, 10,* 253–257, 1986.

Merilees, P. E. and Warn, H., On energy and entropy exchanges in two-dimensional non-divergent flow, *J. Fluid Mech., 69,* 625–630, 1975.

Mikhailovsky, A. B., Nazarenko, S. V., Novakovsky, S. V., Churikov, A. P., and Onistchenko, O. G., Kolmogorov weakly turbulent spectra of some types of drift waves in plasmas, *Phys. Lett., A133,* 407–409, 1988.

Mirabel, A. P., On the effects of triad-resonance interaction of rossby waves in the ocean, *Oceanology, 25,* 558–562, 1985.

Monin, A. S., *Theoretical Geophysical Fluid Dynamics,* Kluwer Academic Publishers, Dordrecht, 1990.

Monin, A. S. and Yaglom, A. M., *Statistical Fluid Mechanics,* MIT Press, Cambridge, Mass., vol. 1, 1971; vol. 2, 1975.

Panetta, R. L., Zonal jets in wide baroclinically unstable regions: persistence and scale selection, *J. Atm. Sci., 50,* 2073–2106, 1993.

Pedlosky, J., *Geophysical Fluid Dynamics,* Springer-Verlag, Heidelberg, 1985.

Pelinovsky, Y. N., Wavelike turbulence on a β-plane, *Oceanology, 18,* 187–193, 1977.

Phillips, O. M., *The dynamics of the upper ocean,* University Press, Cambridge, 1966.

Reznik, G. M., On the energy transfer equation for weakly interacting waves, *Int. J. Nonlin. Mech., 19,* 95–113, 1984.

Reznik, G. M., Weak turbulence on a β-plane, in *Synoptic eddies in the ocean,* pp. 73–108, D.Reidel Publishing Company, Dordrecht, Holland, 1986.

Reznik, G. M. and Kozlov, O. V., Weakly nonlinear interactions of Rossby waves in a barotropic ocean, *Izvestiya, USSR Academy of Sci., Atmospheric and Oceanic Physics, 17,* 462–466, 1981.

Reznik, G. M. and Soomere, T., On a method for solving the kinetic equation for Rossby waves, *Proc. Estonian Acad. Sci. Phys. Math., 32,* 294–299, 1983a.

Reznik, G. M. and Soomere, T., On generalized spectra of weakly nonlinear Rossby waves, *Oceanology, 23,* 692–694, 1983b.

Reznik, G. M. and Soomere, T., Numerical investigation of the spectral evolution of weakly nonlinear Rossby waves, *Oceanology, 24,* 287–294, 1984a.

Reznik, G. M. and Soomere, T., On the evolution of an ensemble of Rossby waves to an anisotropic equilibrium state, *Oceanology, 24,* 424–429, 1984b.

Reznik, G. M., Piterbarg, L. I., and Kartashova, E. A., Nonlinear interactions of spherical Rossby modes, *Dyn. Atm. Oceans, 18,* 235–252, 1993.

Rhines, P. B., Waves and turbulence on a β-plane, *J. Fluid Mech., 69,* 417–443, 1975.

Rhines, P. B., The dynamics of unsteady currents, in *The Sea,* vol. 6, pp. 189–318, Wiley, 1977.

Rhines, P. B., Geostrophic turbulence, *Ann. Rev. Fluid Mech., 11,* 401–441, 1979.

Rhines, P. B., Vorticity dynamics of the oceanic general circulation, *Ann. Rev. Fluid Mech., 18,* 433–497, 1986.

Salmon, R., Baroclinic instability and geostrophic turbulence, *Geophys. Astrophys. Fluid Dyn., 15,* 167–211, 1980.

Salmon, R., Holloway, G., and Hendershott, M. C., The equilibrium statistical mechanics of simple quasi-geostrophic models, *J. Fluid Mech., 75,* 691–703, 1976.

Sazontov, A. G., *On the theory of two-dimensional turbulence,* Preprint. Institute of Applied Physics, USSR Acad. Sci., Moscow, 1981.

Sazontov, A. G., Anisotropic spectra of wavelike turbulence on a β-plane, in *USSR symposion 'Fine structure and synoptic variability of seas and oceans'. Extended abstracts,* pp. 147–152, Tallinn, Estonia, Estonian Acad. Sci., 1983.

Soomere, T., Generalized stationary solutions of the kinetic equation of barotropic Rossby waves, *Oceanology, 27,* 407–409, 1987.

Soomere, T., Geometry of the double resonance of Rossby waves, *Ann. Geophys., 10,* 741–748, 1992.

Soomere, T., Double resonance and kinetic equation for Rossby waves, *Ann. Geophys*, *11*, 90–98, 1993.

Soomere, T. and Rannat, K., On the evolution of the energy spectrum of weak geostrophic turbulence on the β-plane, in *Proc. of the XVI Conference of Baltic Oceanographers, Norrköping 4-7 Sept. 1990*, pp. 563–575, Norrköping, Sweden, SMHI, 1990.

Soomere, T. and Rannat, K., Numerical scheme for solving the kinetic equation for Rossby waves in two-layer ocean, *Oceanology*, *31*, 129-134, 1991.

Tapp, M. C., Kinetic equations for 2-d turbulent flow, *Quart. J. R. Met. Soc.*, *115*, 173–199, 1989.

Vallis, G. K., On the predictability of quasi-geostrophic flow: the effects of beta and baroclinicity, *J. Atm. Sci.*, *40*, 10–27, 1983.

Vallis, G. K. and Maltrud, M. E., Generation of mean flows and jets on a beta plane and over topography, *J. Phys. Oceanogr.*, *23*, 1346–1362, 1993.

Williams, P. G., Planetary circulations: 1. barotropic representation of Jovian and terrestrial turbulence, *J. Atm Sci.*, *35*, 1399–1426, 1978.